PHYSICAL REVIEW D **91,** 074025 (2015)

Light axial vector mesons

Kan Chen,[1,2,*] Cheng-Qun Pang,[1,2,†] Xiang Liu,[1,2,‡,§] and Takayuki Matsuki[3,4,1,‖]

[1]*School of Physical Science and Technology, Lanzhou University, Lanzhou 730000, China*

[2]*Research Center for Hadron and CSR Physics, Lanzhou University Institute of Modern Physics of CAS, Lanzhou 730000, China*

[3]*Tokyo Kasei University, 1-18-1 Kaga, Itabashi, Tokyo 173-8602, Japan*

[4]*Theoretical Research Division, Nishina Center, RIKEN, Saitama 351-0198, Japan*

(Received 1 February 2015; published 22 April 2015)

Inspired by the abundant experimental observation of axial-vector states, we study whether the observed axial-vector states can be categorized into the conventional axial-vector meson family. In this paper we carry out an analysis based on the mass spectra and two-body Okubo-Zweig-Iizuka-allowed decays. Besides testing the possible axial-vector meson assignments, we also predict abundant information for their decays and the properties of some missing axial-vector mesons, which are valuable for further experimental exploration of the observed and predicted axial-vector mesons.

DOI: 10.1103/PhysRevD.91.074025 PACS numbers: 14.40.Be, 12.38.Lg, 13.25.Jx

I. INTRODUCTION

Among the light unflavored mesons listed in the Particle Data Group (PDG) [1], there are abundant light axial-vector mesons with a spin-parity quantum number $J^P = 1^+$, which form a P-wave meson family. Usually, we adopt h_1, b_1, f_1, and a_1 to express the corresponding states with the quantum numbers $I^G(J^{PC}) = 0^-(1^{+-})$, $1^+(1^{+-})$, $0^+(1^{++})$, and $1^-(1^{++})$, respectively. In Table I, we collect the experimental information on the observed h_1, b_1, f_1, and a_1 states, as well as the corresponding resonance parameters and the observed decay channels.

Facing so many axial-vector states in the PDG, we need to examine whether all of these states can be categorized into the axial-vector meson family, which is crucial for revealing their underlying structures. We also notice that most axial-vector states are either omitted by the PDG or are recent findings needing confirmation. Due to the unclear experimental status of light axial-vector states, we need to carry out a quantitative investigation of them, which would be helpful for further experimental studies, especially of those axial-vector states either omitted by the PDG or unconfirmed by other experiments.

In this work, we carry out a systematic study of the axial-vector states by analyzing mass spectra and Okubo-Zweig-Iizuka (OZI)-allowed two-body strong decay behaviors. Our investigations are based on the assumption that all of the axial mesons can be explained within the conventional $q\bar{q}$ picture. Comparing our numerical results with the experimental data, we can further test the possible assignments of the states in the axial-vector meson family. In addition, information on the predicted decays of the axial-vector states observed or still missing in experiments is valuable to further experimental study of axial-vector meson.

This paper is organized as follows. In Sec. II, we present the phenomenological analysis by combining our theoretical results with the corresponding experimental data; the Regge trajectory analysis is adopted to study mass spectra of the axial-vector meson family and the quark-pair creation (QPC) model is applied to calculate their OZI-allowed strong decay behavior. Finally, the discussion and conclusion are given in Sec. III.

II. PHENOMENOLOGICAL STUDY OF OBSERVED AXIAL-VECTOR STATES

A Regge trajectory analysis is an effective approach to study a meson spectrum [31], especially a light-meson spectrum. The masses and radial quantum numbers of light mesons with the same quantum number satisfy the following relation:

$$M^2 = M_0^2 + (n-1)\mu^2, \tag{1}$$

where M_0 and M are the masses of the ground state and the corresponding radial excitation with radial quantum number n, respectively. μ^2 denotes the slope of the trajectory with a universal $\mu^2 = 1.25 \pm 0.15\ \mathrm{GeV}^2$ [31].

In Fig. 1, we present the Regge trajectory analysis, in which we consider all of the axial-vector states listed in the PDG as shown in Table I. Besides the observed ones, we also predict some missing states and show them in Fig. 1. Additionally, we notice that there are two possible candidates for the a_1 meson with quantum number $n^{2s+1}J_L = 3^3P_1$, i.e., $a_1(1930)$ and $a_1(2095)$. On the other hand, both $f_1(1420)$ and $f_1(1510)$ can be an $s\bar{s}$ partner of $f_1(1285)$ by analyzing only the Regge trajectory. Thus, a

*chenk_10@lzu.edu.cn
†pangchq13@lzu.edu.cn
‡Corresponding author
§xiangliu@lzu.edu.cn
‖matsuki@tokyo-kasei.ac.jp

TABLE I. Resonance parameters and strong decay channels of the axial-vector states collected in the PDG [1]. The masses and widths are average values taken from the PDG. The states omitted from the PDG summary table are marked by a superscript ♮, while the states listed as further states in the PDG are marked by a superscript ♭.

$I^G(J^{PC})$	State	Mass (MeV)	Width (MeV)	The observed decay channels
	$a_1(1260)$	1230 ± 40	$250 \sim 600$	3π [2], $\pi\rho$ [3], $\sigma\pi$ [4]
	$a_1(1640)^\natural$	1647 ± 22	254 ± 27	3π [5], $\pi\rho$ [4,6], $\sigma\pi$ [5], $f_2(1270)\pi$ [5]
$1^-(1^{++})$	$a_1(1930)^\flat$	1930^{+30}_{-70}	155 ± 45	$3\pi^0$ [7]
	$a_1(2095)^\flat$	$2096 \pm 17 \pm 121$	$451 \pm 41 \pm 81$	$\pi^+\pi^-\pi^-$ [8]
	$a_1(2270)^\flat$	2270^{+55}_{-40}	305^{+70}_{-40}	$3\pi^0$ [7]
	$b_1(1235)$	1229.5 ± 3.2	142 ± 9	$\omega\pi$ [9–11]
$1^+(1^{+-})$	$b_1(1960)^\flat$	1960 ± 35	345 ± 75	$\omega\pi^0$ [12]
	$b_1(2240)^\flat$	2240 ± 35	320 ± 85	$\omega\pi^0$ [12]
	$f_1(1285)$	1282.1 ± 0.6	24.2 ± 1.1	$\rho^0\rho^0$ [13], $\eta\pi\pi$ [14–16], $a_0\pi$ [15–17], $K\bar{K}\pi$ [15,16,18]
	$f_1(1420)$	1426.4 ± 0.9	54.9 ± 2.6	$K\bar{K}\pi$ [19,20], $K\bar{K}^*(892)+$ c.c [18–20]
$0^+(1^{++})$	$f_1(1510)^\natural$	1518 ± 5	73 ± 25	$K\bar{K}^*(892)+$ c.c [21,22], $\pi^+\pi^-\eta'$ [23]
	$f_1(1970)^\flat$	1971 ± 15	240 ± 45	$\eta\pi^0\pi^0$ [24]
	$f_1(2310)^\flat$	2310 ± 60	255 ± 70	$\eta\pi^0\pi^0$ [24]
	$h_1(1170)$	1170 ± 20	360 ± 40	$\pi\rho$ [25–27]
	$h_1(1380)^\natural$	1386 ± 19	91 ± 30	$K\bar{K}^*(892)+$ c.c [21,28]
$0^-(1^{+-})$	$h_1(1595)^\natural$	$1594 \pm 15^{+10}_{-60}$	$384 \pm 60^{+70}_{100}$	$\omega\eta$ [29]
	$h_1(1965)^\flat$	1965 ± 45	345 ± 75	$\omega\eta$ [30]
	$h_1(2215)^\flat$	2215 ± 40	325 ± 55	$\omega\eta$ [30]

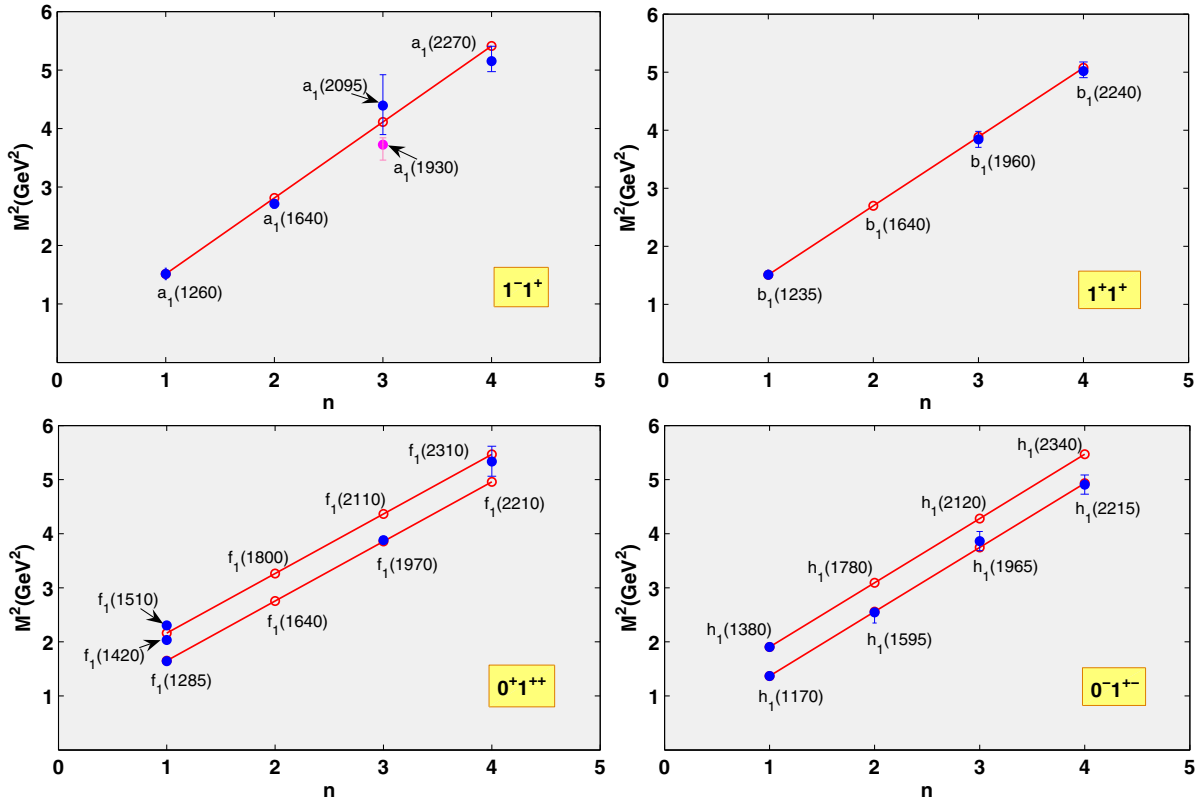

FIG. 1 (color online). Regge trajectory analysis for a_1, b_1, f_1, and h_1 with typical $\mu^2 = 1.30$ GeV^2, 1.19 GeV^2, 1.10 GeV^2, and 1.19 GeV^2, respectively, which can be covered by $\mu^2 = 1.25 \pm 0.15$ GeV^2 given in Ref. [31]. The experimental errors of discussed axial-vector states are given, which are taken from the PDG [1]. Here, ◦ and • denote theoretical and experimental values, respectively.

TABLE II. OZI-allowed two-body decay channels for a_1 and h_1 states marked by $\surd$. Here, ρ, ω, and η denote $\rho(770)$, $\omega(782)$, and $\eta(548)$, respectively. The axial-vector states predicted by the Regge trajectory analysis are marked by a superscript $\natural$.

Channel	$a_1(1260)$	$a_1(1640)$	$a_1(1930)$	$a_1(2095)$	$a_1(2270)$	Channel	$h_1(1170)$	$h_1(1380)$	$h_1(1595)$	$h_1^\natural(1780)$	$h_1(1965)$	$h_1^\natural(2120)$	$h_1(2215)$	$h_1^\natural(2340)$
$\pi\rho$	$\surd$	$\surd$	$\surd$	$\surd$	$\surd$	$\pi\rho$	$\surd$	$\surd$	$\surd$	$\surd$	$\surd$	$\surd$	$\surd$	$\surd$
$\sigma\pi$	$\surd$	$\surd$	$\surd$	$\surd$	$\surd$	KK^*		$\surd$	$\surd$	$\surd$	$\surd$	$\surd$	$\surd$	$\surd$
πf_0	$\surd$	$\surd$	$\surd$	$\surd$	$\surd$	$\eta\omega$		$\surd$	$\surd$	$\surd$	$\surd$	$\surd$	$\surd$	$\surd$
$\pi f_1(1420)$		$\surd$	$\surd$	$\surd$	$\surd$	$\omega\sigma$			$\surd$	$\surd$	$\surd$	$\surd$	$\surd$	$\surd$
$\pi\rho(1450)$		$\surd$	$\surd$	$\surd$	$\surd$	$KK_1(1270)$				$\surd$	$\surd$	$\surd$	$\surd$	$\surd$
$\rho\omega$		$\surd$	$\surd$	$\surd$	$\surd$	$\omega\eta'(958)$				$\surd$	$\surd$	$\surd$	$\surd$	$\surd$
$\eta a_0(980)$		$\surd$	$\surd$	$\surd$	$\surd$	ωf_0				$\surd$	$\surd$	$\surd$	$\surd$	$\surd$
KK^*		$\surd$	$\surd$	$\surd$	$\surd$	$\rho a_0(980)$				$\surd$	$\surd$	$\surd$	$\surd$	$\surd$
$\pi b_1(1235)$		$\surd$	$\surd$	$\surd$	$\surd$	$\pi\rho(1450)$				$\surd$	$\surd$	$\surd$	$\surd$	$\surd$
$\pi f_2(1270)$		$\surd$	$\surd$	$\surd$	$\surd$	$KK_1(1400)$					$\surd$	$\surd$	$\surd$	$\surd$
$\pi f_1(1285)$		$\surd$	$\surd$	$\surd$	$\surd$	$KK^*(1410)$					$\surd$	$\surd$	$\surd$	$\surd$
$\rho a_0(980)$			$\surd$	$\surd$	$\surd$	$KK_0^*(1430)$					$\surd$	$\surd$	$\surd$	$\surd$
$KK_1(1400)$			$\surd$	$\surd$	$\surd$	$KK_2^*(1430)$					$\surd$	$\surd$	$\surd$	$\surd$
$\eta a_1(1260)$			$\surd$	$\surd$	$\surd$	K^*K^*					$\surd$	$\surd$	$\surd$	$\surd$
$\pi\rho(1700)$			$\surd$	$\surd$	$\surd$	$\eta\omega(1420)$					$\surd$	$\surd$	$\surd$	$\surd$
$KK_1(1270)$			$\surd$	$\surd$	$\surd$	$\sigma h_1(1170)$					$\surd$	$\surd$	$\surd$	$\surd$
$KK^*(1410)$			$\surd$	$\surd$	$\surd$	$\pi\rho(1700)$					$\surd$	$\surd$	$\surd$	$\surd$
$KK_0^*(1430)$			$\surd$	$\surd$	$\surd$	$\rho a_2(1320)$						$\surd$	$\surd$	$\surd$
$KK_2^*(1430)$			$\surd$	$\surd$	$\surd$	$\omega f_2(1270)$						$\surd$	$\surd$	$\surd$
K^*K^*			$\surd$	$\surd$	$\surd$	$\sigma\omega(1420)$						$\surd$	$\surd$	$\surd$
$\eta a_2(1320)$			$\surd$	$\surd$	$\surd$	$\omega f_1(1285)$						$\surd$	$\surd$	$\surd$
$\sigma a_1(1260)$			$\surd$	$\surd$	$\surd$	$\rho\pi(1300)$						$\surd$	$\surd$	$\surd$
$\sigma a_2(1320)$			$\surd$	$\surd$	$\surd$	$\rho a_1(1260)$						$\surd$	$\surd$	$\surd$
$\rho\pi(1300)$				$\surd$	$\surd$	$K^*K_1(1270)$							$\surd$	$\surd$
$\eta a_0(1450)$				$\surd$	$\surd$	$f_0 h_1(1170)$							$\surd$	$\surd$
$\omega b_1(1235)$				$\surd$	$\surd$	$KK^*(1680)$							$\surd$	$\surd$
$\rho h_1(1170)$				$\surd$	$\surd$	$\omega f_1(1420)$							$\surd$	$\surd$
$\rho a_1(1260)$				$\surd$	$\surd$	$K^*K_1(1400)$								$\surd$
$K^*K_1(1270)$					$\surd$									
$\rho a_2(1320)$					$\surd$									
$\rho\omega(1420)$					$\surd$									
$\rho a_0(1450)$					$\surd$									
$KK^*(1680)$					$\surd$									
$\eta'(958)a_0(980)$					$\surd$									

TABLE III. OZI-allowed two-body decay channels for b_1 and f_1 states marked by $\surd$. Here, ρ, ω, and η denote $\rho(770)$, $\omega(782)$, and $\eta(548)$, respectively. The axial-vector states predicted by the Regge trajectory analysis are marked by a superscript $\natural$.

Channel	$b_1(1235)$	$b_1^\natural(1640)$	$b_1(1960)$	$b_1(2240)$	Channel	$f_1(1285)$	$f_1(1420)$	$f_1(1510)$	$f_1^\natural(1640)$	$f_1^\natural(1800)$	$f_1(1970)$	$f_1^\natural(2110)$	$f_1^\natural(2210)$	$f_1(2310)$
$\pi\omega$	$\surd$	$\surd$	$\surd$	$\surd$	$\pi a_0(980)$	$\surd$	$\surd$	$\surd$	$\surd$	$\surd$	$\surd$	$\surd$	$\surd$	$\surd$
$\pi a_0(980)$	$\surd$	$\surd$	$\surd$	$\surd$	$\sigma\eta$	$\surd$	$\surd$	$\surd$	$\surd$	$\surd$	$\surd$	$\surd$	$\surd$	$\surd$
$\pi a_1(1260)$		$\surd$	$\surd$	$\surd$	$\pi a_1(1260)$		$\surd$	$\surd$	$\surd$	$\surd$	$\surd$	$\surd$	$\surd$	$\surd$
$\pi a_2(1320)$		$\surd$	$\surd$	$\surd$	KK^*		$\surd$	$\surd$	$\surd$	$\surd$	$\surd$	$\surd$	$\surd$	$\surd$
$\pi\omega(1420)$		$\surd$	$\surd$	$\surd$	$\pi a_2(1320)$			$\surd$	$\surd$	$\surd$	$\surd$	$\surd$	$\surd$	$\surd$
$\pi a_0(1450)$		$\surd$	$\surd$	$\surd$	$\pi a_0(1450)$				$\surd$	$\surd$	$\surd$	$\surd$	$\surd$	$\surd$
$\eta\rho$		$\surd$	$\surd$	$\surd$	ηf_0				$\surd$	$\surd$	$\surd$	$\surd$	$\surd$	$\surd$
$\rho\rho$		$\surd$	$\surd$	$\surd$	$\rho\rho$				$\surd$	$\surd$	$\surd$	$\surd$	$\surd$	$\surd$
KK^*		$\surd$	$\surd$	$\surd$	$\omega\omega$				$\surd$	$\surd$	$\surd$	$\surd$	$\surd$	$\surd$
$\sigma\rho$		$\surd$	$\surd$	$\surd$	$\sigma\eta'$				$\surd$	$\surd$	$\surd$	$\surd$	$\surd$	$\surd$
$\eta'(958)\rho$			$\surd$	$\surd$	$KK_1(1270)$					$\surd$	$\surd$	$\surd$	$\surd$	$\surd$
ρf_0			$\surd$	$\surd$	K^*K^*					$\surd$	$\surd$	$\surd$	$\surd$	$\surd$
$\omega a_0(980)$			$\surd$	$\surd$	$\omega h_1(1170)$						$\surd$	$\surd$	$\surd$	$\surd$
$KK_1(1270)$			$\surd$	$\surd$	$\eta'(958)f_0$						$\surd$	$\surd$	$\surd$	$\surd$
$KK_1(1400)$			$\surd$	$\surd$	$\eta f_2(1270)$						$\surd$	$\surd$	$\surd$	$\surd$
$KK_0^*(1410)$			$\surd$	$\surd$	$KK_1(1400)$						$\surd$	$\surd$	$\surd$	$\surd$
$KK_0^*(1430)$			$\surd$	$\surd$	$KK^*(1410)$						$\surd$	$\surd$	$\surd$	$\surd$
$KK_2^*(1430)$			$\surd$	$\surd$	$KK_0^*(1430)$						$\surd$	$\surd$	$\surd$	$\surd$
$\sigma b_1(1235)$			$\surd$	$\surd$	$KK_2^*(1430)$						$\surd$	$\surd$	$\surd$	$\surd$
K^*K^*			$\surd$	$\surd$	$\eta f_1(1285)$						$\surd$	$\surd$	$\surd$	$\surd$
$\omega a_2(1320)$				$\surd$	$\sigma f_2(1270)$						$\surd$	$\surd$	$\surd$	$\surd$
$\omega\pi(1300)$				$\surd$	$\sigma f_1(1285)$						$\surd$	$\surd$	$\surd$	$\surd$
$K^*K_1(1270)$				$\surd$	$\sigma f_1(1420)$							$\surd$	$\surd$	$\surd$
$\eta\rho(1450)$				$\surd$	$\rho b_1(1235)$							$\surd$	$\surd$	$\surd$
$KK^*(1680)$				$\surd$	$\eta f_1(1420)$							$\surd$	$\surd$	$\surd$
$a_0(980)h_1(1170)$				$\surd$	$\omega\omega(1420)$								$\surd$	$\surd$
$\rho f_2(1270)$				$\surd$	$K^*K_1(1270)$								$\surd$	$\surd$
$\rho f_1(1285)$				$\surd$	$KK^*(1680)$									$\surd$
$\rho f_1(1420)$				$\surd$	$f_0f_2(1270)$									$\surd$
$\rho b_1(1235)$				$\surd$	$f_0f_1(1285)$									$\surd$
$\omega a_1(1260)$				$\surd$	$a_0(980)a_1(1260)$									$\surd$
					$a_0(980)\pi(1300)$									$\surd$
					$a_0(980)a_2(1320)$									$\surd$
					$\eta'(958)f_2(1270)$									$\surd$
					$\rho\rho(1450)$									$\surd$
					$\eta'(958)f_1(1285)$									$\surd$
					$K^*K_1(1400)$									$\surd$

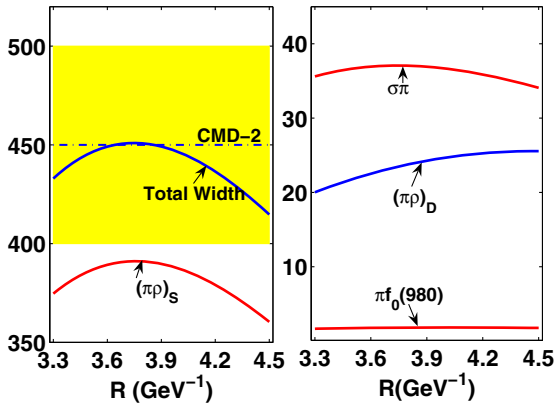

FIG. 2 (color online). Total and partial decay widths of $a_1(1260)$ depending on R. Here, the dot-dashed line with the band is taken from the experimental data from Ref. [62]. The S-wave and D-wave contributions to the decay width of $a_1(1260) \to \pi\rho$ are also given separately. All results are in units of MeV.

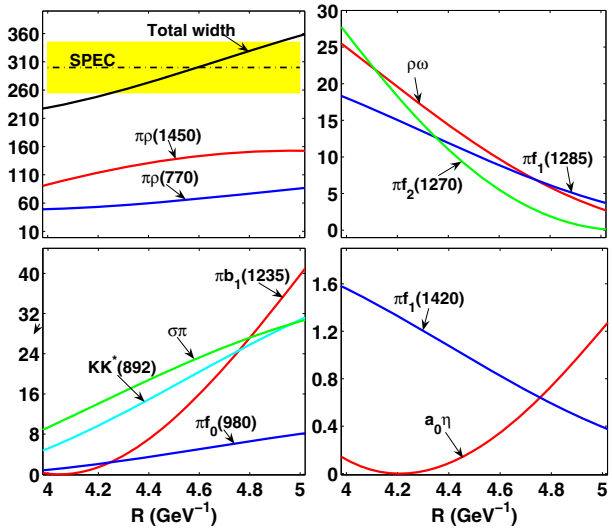

FIG. 3 (color online). R dependence of the decay behaviors of $a_1(1640)$. Here, the dot-dashed line with the band is the experimental total width from Ref. [5]. All results are in units of MeV.

further study of their strong decay behaviors would help to test these possible assignments to the observed axial-vector states and could provide more predictions of the observed and still-missing axial-vector mesons, which are valuable for the future experimental exploration of axial-vector mesons.

To obtain the decay behaviors of the axial-vector mesons, we adopt the QPC model, which was first proposed by Micu [32] and further developed by the Orsay group [33–37]. This model was widely applied to study the OZI-allowed two-body strong decay of hadrons [38–59]. In the following, we briefly introduce the QPC model.

For a decay process $A \to B + C$, we can write

$$\langle BC|\mathcal{T}|A\rangle = \delta^3(\mathbf{P}_B + \mathbf{P}_C)\mathcal{M}^{M_{J_A}M_{J_B}M_{J_C}}, \tag{2}$$

where $\mathbf{P}_{B(C)}$ is a three-momentum of a meson $B(C)$ in the rest frame of a meson A. A subscript $M_{J_i}(i = A, B, C)$ denotes an orbital magnetic momentum. The transition operator $\mathcal{T}$ is introduced to describe a quark-antiquark pair creation from vacuum, which has the quantum number $J^{PC} = 0^{++}$, i.e., $\mathcal{T}$ can be expressed as

$$\mathcal{T} = -3\gamma\sum_m \langle 1m; 1-m|00\rangle \int d\mathbf{p}_3 d\mathbf{p}_4 \delta^3(\mathbf{p}_3 + \mathbf{p}_4) \times \mathcal{Y}_{1m}\left(\frac{\mathbf{p}_3 - \mathbf{p}_4}{2}\right)\chi^{34}_{1,-m}\phi^{34}_0(\omega^{34}_0)_{ij}b^\dagger_{3i}(\mathbf{p}_3)d^\dagger_{4j}(\mathbf{p}_4), \tag{3}$$

which is constructed in a completely phenomenological way to reflect the creation of a quark-antiquark pair from vacuum, where the quark and antiquark are denoted by indices 3 and 4, respectively. As a dimensionless parameter, γ depicts the strength of the creation of $q\bar{q}$ from vacuum,

TABLE IV. Some typical ratios of decay widths of $a_1(1260)$. The $\Gamma(\pi\rho)_{S(D)}$ represent the $S(D)$-wave decay width of $a_1(1260) \to \pi\rho$.

	Our work	Experimental data
$\Gamma((\pi\rho)_S)/\Gamma_{\text{Total}}$	0.86	0.60 [3]
$\Gamma((\pi\rho)_D)/\Gamma_{\text{Total}}$	5.3×10^{-2}	$(1.30 \pm 0.60 \pm 0.22) \times 10^{-2}$ [3]
$\Gamma_{\pi\sigma}/\Gamma_{\text{Total}}$	8.2×10^{-2}	$(18.76 \pm 4.29 \pm 1.48) \times 10^{-2}$ [3]
$\Gamma_{\sigma\pi}/\Gamma_{(\rho\pi)_S}$	0.09	0.06 ± 0.05 [1]

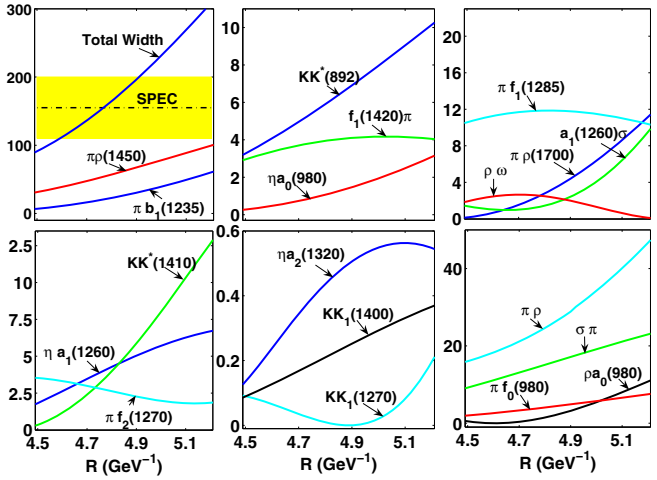

FIG. 4 (color online). R dependence of the calculated partial and total decay widths of $a_1(1930)$. Here, the dot-dashed line with the band is the experimental total width from Ref. [7]. All results are in units of MeV.

TABLE V. Typical ratios of the decay widths of $a_1(1640)$ corresponding to the R range (4.30–4.64) GeV^{-1}.

Ratio	Value	Ratio	Value
$\Gamma_{\pi\rho}/\Gamma_{\rm Total}$	0.216–0.227	$\Gamma_{\pi\rho(1450)}/\Gamma_{\rm Total}$	0.473–0.474
$\Gamma_{\pi b_1(1235)}/\Gamma_{\rm Total}$	0.014–0.059	$\Gamma_{KK^*}/\Gamma_{\sigma\pi}$	0.166–0.221
$\Gamma_{\pi f_2(1270)}/\Gamma_{\rho\omega}$	0.523–0.855	$\Gamma_{\pi f_1(1420)}/\Gamma_{\pi f_1(1285)}$	0.089–0.094
$\Gamma_{\pi f_0}$	0.166–0.221		

where $\gamma = 8.7$ and $8.7/\sqrt{3}$ [51] corresponds to the $u\bar{u}/d\bar{d}$ and $s\bar{s}$ creations, respectively. $\mathcal{Y}_{\ell m}(\mathbf{p}) = |\mathbf{p}|^{\ell} Y_{\ell m}(\mathbf{p})$ is the solid harmonic. χ, ϕ, and ω denote the spin, flavor, and color wave functions, which can be treated separately. In addition, i and j denote the color indices of a $q\bar{q}$ pair.

By the Jacob-Wick formula [60], the decay amplitude is expressed as

$$\mathcal{M}^{JL}(\mathbf{P}) = \frac{\sqrt{4\pi(2L+1)}}{2J_A+1} \sum_{M_{J_B}M_{J_C}} \langle L0; JM_{J_A}|J_A M_{J_A}\rangle \times \langle J_B M_{J_B}; J_C M_{J_C}|J_A M_{J_A}\rangle \mathcal{M}^{M_{J_A}M_{J_B}M_{J_C}}, \quad (4)$$

and the general decay width reads

$$\Gamma = \frac{\pi}{4}\frac{|\mathbf{P}|}{m_A^2}\sum_{J,L}|\mathcal{M}^{JL}(\mathbf{P})|^2, \quad (5)$$

where m_A is the mass of an initial state A. We use the simple harmonic oscillator wave function to describe the space wave function of mesons, which has the following expression:

TABLE VI. Typical ratios for $a_1(1930)$ and $a_1(2095)$. The R ranges are (4.58–4.92) GeV^{-1} and (4.78–5.16) GeV^{-1} for $a_1(1930)$ and $a_1(2095)$, respectively.

Ratio	$a_1(1930)$	$a_1(2095)$
$\Gamma_{\pi\rho}/\Gamma_{\rm Total}$	0.151–0.162	0.139–0.176
$\Gamma_{\pi b_1(1235)}/\Gamma_{\rm Total}$	0.092–0.160	0.206–0.2542
$\Gamma_{\pi\rho(1700)}/\Gamma_{\rm Total}$	0.005–0.024	0.039–0.0529
$\Gamma_{\sigma\pi}/\Gamma_{\rm Total}$	0.088–0.097	0.058–0.073
$\Gamma_{\pi\rho(1450)}/\Gamma_{\rm Total}$	0.339–0.347	0.189–0.253
$\Gamma_{\pi b_1(1235)}/\Gamma_{\pi\rho(1450)}$	0.271–0.462	0.348–1.813
$\Gamma_{\eta a_1(1260)}/\Gamma_{KK^*(892)}$	0.629–0.719	1.141–1.742
$\Gamma_{\rho\omega}\Gamma_{\pi f_2(1270)}$	0.705–0.850	0.188–0.451
$\Gamma_{\eta a_0(980)}/\Gamma_{\pi\rho(1700)}$	0.317–0.809	0.239–0.279
$\Gamma_{KK_1(1400)}/\Gamma_{\eta a_2(1320)}$	0.508–0.553	1.693–4.846
$\Gamma_{KK_1(1400)}/\Gamma_{\rho a_0(980)}$	⋯	0.145–0.184
$\Gamma_{\eta a_0(1450)}/\Gamma_{KK_0^*(1430)}$	⋯	0.206–0.838

$$\Psi_{nlm}(R,\mathbf{p}) = \mathcal{R}_{nl}(R,\mathbf{p})\mathcal{Y}_{lm}(\mathbf{p}), \quad (6)$$

where the concrete values of the parameter R involved in our calculation are given in Ref. [61] for the ground states. However, its value is to be fixed for each excited state.

With the above preparation, we further discuss the OZI-allowed decay behaviors of the axial-vector mesons. The allowed decay modes are listed in Tables II and III.

A. a_1 states

The Regge trajectory analysis indicates that $a_1(1260)$ can be regarded as a ground state. The obtained total and

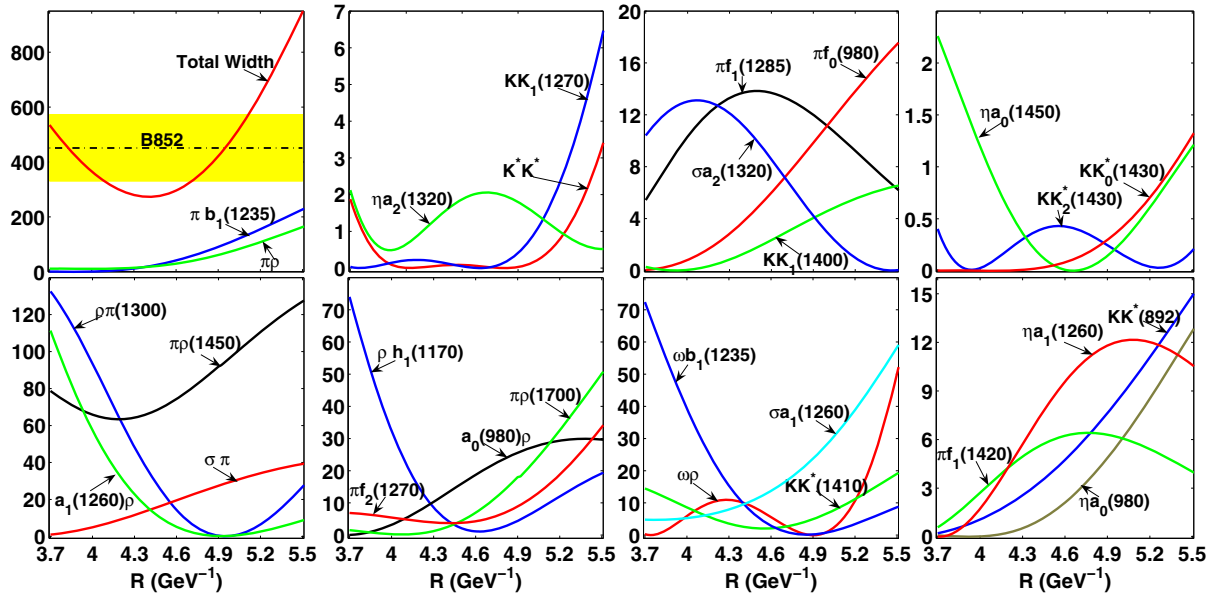

FIG. 5 (color online). R dependence of the calculated partial and total decay widths of $a_1(2095)$. Here, the dot-dashed line with the band is the experimental total width from Ref. [7]. All results are in units of MeV.

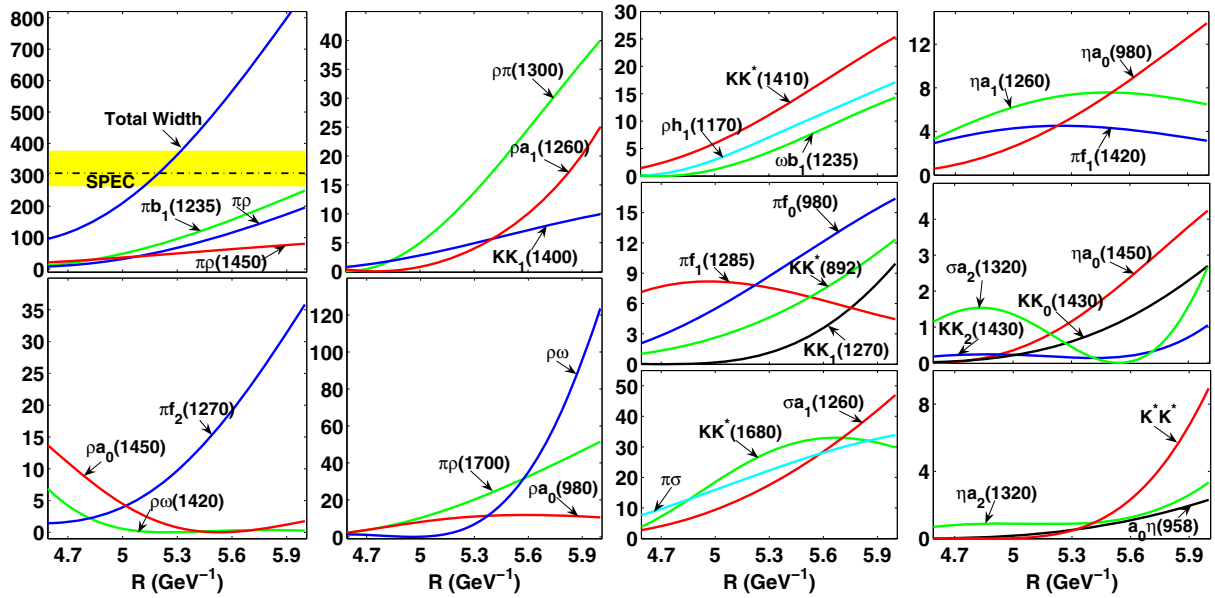

FIG. 6 (color online). R dependence of the calculated partial and total decay widths of $a_1(2270)$. Here, the dot-dashed line with the band is the experimental total width from Ref. [7]. All results are in units of MeV.

partial decay widths of $a_1(1260)$ are listed in Fig. 2, which shows that $\pi\rho$ is the dominant channel. In Fig. 2, we give the partial decay widths of $a_1(1260) \to \pi\rho$ from the S-wave and D-wave contributions. Here, the D-wave/S-wave amplitude ratio in the decay $a_1(1260) \to \pi\rho$ is -0.248 with a typical value of $R = 3.846\ \mathrm{GeV}^{-1}$ [61] in our calculation, which is comparable with the B852 data $(-0.14 \pm 0.04 \pm 0.07)$ [4]. Our result also shows that $a_1(1260) \to f_0\pi$ is a subordinate decay mode with the partial decay width 1.82 MeV, which explains why there has been no evidence of $a_1(1260) \to f_0\pi$ in experiments [3]. As shown in Fig. 2, the calculated total width can reproduce the CMD2 data given in Ref. [62]. In addition, we also give some typical ratios relevant to the partial decay and total widths together with the corresponding experimental data in Table IV. In summary, our results are comparable with the experimental values and support $a_1(1260)$ as a ground state in the a_1 meson family.

If $a_1(1640)$ is the first radial excitation of $a_1(1260)$, its decay behavior depending on the R value is shown in Fig. 3. We use the experimental total width [5] and the ratio $\Gamma(f_2(1270)\pi)/\Gamma(\sigma\pi) = 0.24 \pm 0.07$ [5] to get $R = (4.30\text{–}4.64)\ \mathrm{GeV}^{-1}$.[1] The main decay modes of $a_1(1640)$ are $\pi\rho$, $\pi\rho(1450)$, $\pi f_2(1270)$, $\pi f_1(1285)$, and $\rho\omega$. Additionally, we provide further information on the typical ratios of $a_1(1640)$ decays in Table V.

There are two possible candidates for the second radial excitation of $a_1(1260)$. In the following, we discuss the decay behaviors of $a_1(1930)$ and $a_1(2095)$ by combining the corresponding experimental data. In Figs. 4 and 5, we present the R dependence of the decay behaviors of these a_1's, respectively. That is, the obtained total width of $a_1(1930)$ can be fitted with the data from Ref. [7] when $R = 4.58\text{–}4.92\ \mathrm{GeV}^{-1}$, while that of $a_1(2095)$ can overlap with the experimental data [7] when $R = (4.78\text{–}5.16)\ \mathrm{GeV}^{-1}$. Thus, it is difficult to distinguish which a_1 is more suitable as a candidate for the second radial excitation of $a_1(1260)$ by studying only the total decay widths. Besides, we can learn from the Regge trajectory analysis that there is only one state for the 3^3P_1 state, and it is doubtful that both $a_1(1930)$ and $a_1(2095)$ exist, as mentioned in Ref. [7]. However, there exist different behaviors of the partial decay widths of these a_1's. The $a_1(1930)$ mainly decays into final states $\pi\rho$, $\pi\rho(1450)$, and $\pi b_1(1235)$, while the $\pi f_1(1285)$ and $\sigma\pi$ modes also have sizable contributions. The decays of $a_1(1930)$ into $KK_0^*(1430)$, $KK_2^*(1430)$, and $K^*(896)$ $K^*(896)$ have tiny decay widths, which are not listed in Fig. 4. As for $a_1(2095)$, its dominant decay channels are $\pi b_1(1235)$, $\pi\rho$, and $\pi\rho(1450)$ and are shown in Fig. 5. The other decay channels—like $\rho a_0(980)$, $\pi\rho(1700)$, $\pi f_1(1285)$, πf_0, and $\sigma\pi$—also have considerable contributions to the total decay width. In Table VI, we also list some typical ratios relevant to their decays. We still need to emphasize one point. At present, $a_1(1930)$ and $a_1(2095)$ are not well established in experiments. The authors of

[1]Using the experimental total width [5], we find that overlap exists between our theoretical and experimental results when taking $R = 4.26\text{–}4.92\ \mathrm{GeV}^{-1}$. Then, we can further constrain the R values by the ratio $\Gamma(f_2(1270)\pi)/\Gamma(\sigma\pi) = 0.24 \pm 0.07$ [5], where the constrained $R = (4.30\text{–}4.64)\ \mathrm{GeV}^{-1}$, which is adopted to present other typical ratios of $a_1(1640)$.

TABLE VII. Calculated ratios of the decays of $a_1(2270)$. Here, all the results correspond to the R range (5.12–5.32) GeV^{-1}.

Ratio	Value	Ratio	Value
$\Gamma_{\pi\rho}/\Gamma_{\mathrm{Total}}$	0.164–0.184	$\Gamma_{\pi f_1(1285)}/\Gamma_{\pi\sigma}$	0.313–0.435
$\Gamma_{\pi b_1(1235)}/\Gamma_{\mathrm{Total}}$	0.247–0.264	$\Gamma_{KK^*(892)}/\Gamma_{\eta a_1(1260)}$	0.313–0.487
$\Gamma_{\pi\rho_{1700}}/\Gamma_{\mathrm{Total}}$	0.052–0.056	$\Gamma_{\pi f_1(1420)}/\Gamma_{\rho a_0(980)}$	0.404–0.469
$\Gamma_{\sigma\pi}/\Gamma_{\mathrm{Total}}$	0.064–0.070	$\Gamma_{\eta a_0(980)}/\Gamma_{\pi f_2(1270)}$	0.532–0.612
$\Gamma_{\pi\rho(1450)}/\Gamma_{\mathrm{Total}}$	0.134–0.157	$\Gamma_{\eta a_2(1320)}/\Gamma_{\pi f_0}$	0.099–0.131
$\Gamma_{\rho a_1(1260)}/\Gamma_{\omega b_1(1235)}$	0.789–0.926	$\Gamma_{\eta a_0(1450)}/\Gamma_{\omega b_1(1235)}$	0.236–0.273
$\Gamma_{KK_1(1400)}/\Gamma_{\rho\pi_{1300}}$	0.352–0.446	$\Gamma_{\eta a_1(1260)}/\Gamma_{KK^*(1680)}$	0.256–0.297
$\Gamma_{\rho h_1(1170)}/\Gamma_{KK_1(1400)}$	0.573–0.639	$\Gamma_{KK^*(1410)}/\Gamma_{\sigma a_1(1260)}$	0.633–0.638

Ref. [7] indicated that $a_2(1950)$ and $a_1(1930)$ are not securely identified in mass and width, though such contributions are definitely required [7]. However, when considering the Regge trajectory analysis, one finds that the 3^3P_1 state in the a_1 meson family has a mass around 2000 MeV. The two unconfirmed $a_1(1930)$ and $a_1(2095)$ states could be candidates for the 3^3P_1 state in the a_1 meson family, since their masses are close to that of the 3^3P_1 state in the a_1 meson family. Thus, the experimental study of the partial decay widths of $a_1(1930)$ and $a_1(2095)$ will help to reduce the two possible candidates—$a_1(1930)$ and $a_1(2095)$—of the second radial excitation of $a_1(1260)$ to one. In the following, the experimental confirmation of $a_1(1930)$ and $a_1(2095)$ will be crucial for identifying the candidate of the 3^3P_1 state in the a_1 meson family. If $a_1(1930)$ and $a_1(2095)$ cannot be established in experiments, we suggest an experimental search for $a_1(3^3P_1)$; the results for $a_1(3^3P_1)$ predicted in this work would be helpful for such a search.

In Fig. 6, we discuss the decay behavior of $a_1(2270)$ as the third radial excitation of $a_1(1260)$. We find that the main decay mode includes the decay channels $\pi b_1(1235)$, $\pi\rho$, $\pi\rho(1450)$, and $\pi\rho(1700)$. In addition, $KK^*(1410)$, $\rho h_1(1170)$, $KK^*(1680)$, $\pi\sigma$, and $\sigma a_1(1260)$ have important contributions to the total decay width. $\rho a_2(1320)$, $\eta'(958)a_0(980)$, and $K^*K_1(1270)$ are subordinate decay modes, which are not shown in Fig. 6. In Table VII, we also list the typical ratios of the decays of $a_1(2270)$.

B. b_1 states

The Regge trajectory analysis indicates that $b_1(1235)$, $b_1(1960)$, and $b_1(2240)$ are the ground state, second radial excitation, and third radial excitation in the b_1 meson family, respectively. In addition, we also predict a missing $b_1(1640)$ as the first radial excitation. In the following, we study their decays.

As for $b_1(1235)$, there are two allowed decay channels: $\pi\omega$ and $\pi a_0(980)$. The result shown in Fig. 7 shows that the obtained total width overlaps with experimental data from Ref. [63]. Since $b_1 \to \omega\pi$ occurs via S and D waves, we obtain the D-wave/S-wave amplitude ratio of the $b_1 \to \omega\pi$ process, which is 0.465 in our work; this is consistent with the Crystal Barrel data (0.45 ± 0.04) [10]. On the other hand, the decay channel πf_0 has a partial decay width that is less than 1 MeV.

As a predicted b_1 state, $b_1(1640)$ has the decay behavior listed in Fig. 8, where we take the same R range as that for $a_1(1640)$.[2] Its main decay channel is $\pi a_0(980)$, while $\pi a_2(1320)$, $\rho\rho$, $\pi\omega(1420)$, KK^*, and $\omega\pi$ also have considerable contributions to the total decay width. The total decay width is predicted to be 200–232 MeV. Table VIII shows some ratios that are relevant to the decays of $b_1(1640)$, which is valuable for further experimental searches for this axial-vector state.

Assuming that $b_1(1960)$ is the second radial excitation of $b_1(1235)$, we present its total and partial decay widths in Fig. 9. Our calculated total width can cover the experimental data given in Ref. [12]. Its main decay channels are $\pi a_0(1450)$, $\pi\omega$, $\pi a_0(980)$, and $\pi\omega(1420)$, while the partial decay widths of the decay modes $\pi a_1(1260)$, $\rho\eta$, and $\pi a_2(1320)$ are also considerable. We also obtain some ratios of partial decay widths of $b_1(1960)$, which are listed in Table IX.

In Fig. 10, we show the decay behavior of $b_1(2240)$ as the third radial excitation of $b_1(1235)$. Additionally, its main decay modes are $\omega\pi$, $\pi\omega(1420)$, $\pi a_0(980)$, and $\pi a_0(1450)$. Of course, the decay modes $\rho\rho$, $\rho b_1(1235)$, $\pi a_2(1320)$, and $\pi a_1(1260)$ also have obvious contributions to the total decay width. For the convenience of further experimental studies of this state, we provide information on typical ratios of the partial width of $b_1(2240)$ in Table X.

[2]Since $b_1(1640)$ is a predicted state, we take the same R range as that of $a_1(1640)$ to predict the decay behavior of $b_1(1640)$. This treatment is due to the fact that $b_1(1640)$ is the isospin partner of $a_1(1640)$, which has a similar R range.

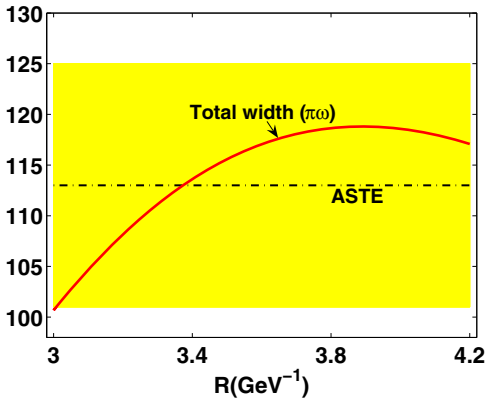

FIG. 7 (color online). R dependence of the calculated total decay width of $b_1(1235)$. Here, the dot-dashed line with the band is the experimental total width from Ref. [63]. The total decay width is in units of MeV.

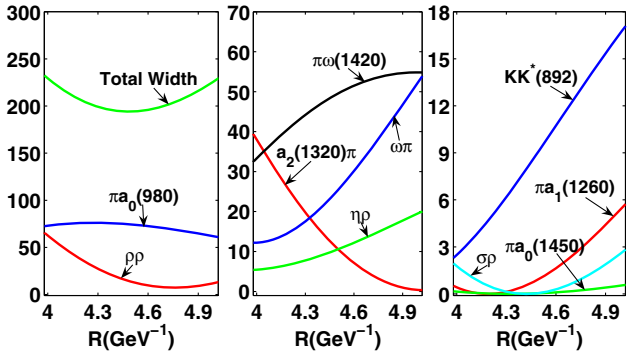

FIG. 8 (color online). R dependence of the calculated partial and total decay widths of $b_1(1640)$. All results are in units of MeV.

C. f_1 states

When discussing f_1 states, we need to consider the admixtures of the flavor wave functions $|n\bar{n}\rangle = (|u\bar{u}\rangle + |d\bar{d}\rangle)/\sqrt{2}$ and $|s\bar{s}\rangle$. $f_1(1285)$ and $f_1(1420)/f_1(1510)$ satisfy

$$\begin{pmatrix} |f_1(1285)\rangle \\ |f_1(1420)/f_1(1510)\rangle \end{pmatrix} = \begin{pmatrix} \cos\phi & -\sin\phi \\ \sin\phi & \cos\phi \end{pmatrix} \begin{pmatrix} |n\bar{n}\rangle \\ |s\bar{s}\rangle \end{pmatrix}, \tag{7}$$

TABLE VIII. Typical ratios for decays of $b_1(1640)$ corresponding to $R = 4.20$–4.90 GeV^{-1}.

Ratio	Value	Ratio	Value
$\Gamma_{\pi a_0(980)}/\Gamma_{\text{Total}}$	0.352–0.368	$\Gamma_{KK^*}/\Gamma_{\omega\pi}$	0.324–0.347
$\Gamma_{\eta\rho}/\Gamma_{\pi\omega(1420)}$	0.164–0.263	$\Gamma_{\pi a_2(1320)}/\Gamma_{\rho\rho}$	0.565–0.681

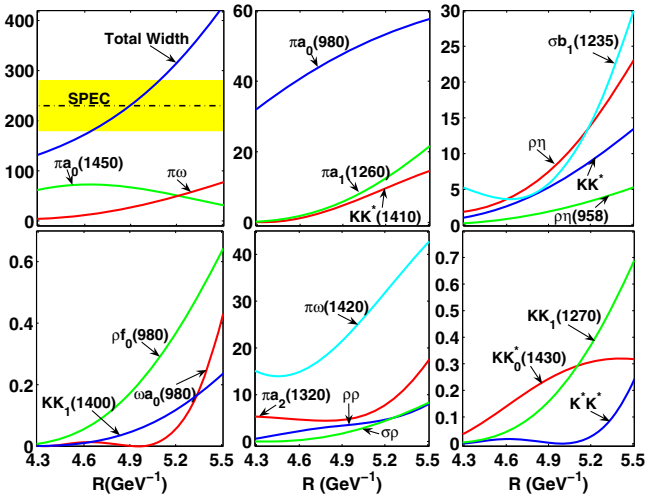

FIG. 9 (color online). R dependence of the calculated partial and total decay widths of $b_1(1960)$. Here, the dot-dashed line with the band is the experimental total width from Ref. [12]. Since the width of the KK_2^* mode is tiny, we do not list its contribution here. All results are in units of MeV.

where both $f_1(1420)$ and $f_1(1510)$ are partners of $f_1(1285)$. (We present their decay behaviors below.) ϕ denotes a mixing angle. This mixing angle was determined in a phenomenological way [64] and is given by $\phi = (20-30)°$, which is consistent with $\phi = (24^{+3.2}_{-2.7})°$ reported by the LHCb Collaboration [65] and $\phi = (21 \pm 5)°$ from the updated lattice QCD analysis [66]. When calculating the decays of $f_1(1285)$ and $f_1(1420)/f_1(1510)$, we take the LHCb value $\phi = 24°$.

In Fig. 1, we have predicted that $f_1(1640)$ is the first radial excitation of $f_1(1285)$ and that $f_1(1800)$ is a partner of $f_1(1640)$; these two predicted axial-vector mesons are related by

$$\begin{pmatrix} |f_1(1640)\rangle \\ |f_1(1800)\rangle \end{pmatrix} = \begin{pmatrix} \cos\phi_1 & -\sin\phi_1 \\ \sin\phi_1 & \cos\phi_1 \end{pmatrix} \begin{pmatrix} |n\bar{n}\rangle \\ |s\bar{s}\rangle \end{pmatrix}. \tag{8}$$

In addition, there exist relations among $f_1(1970)$, the predicted $f_1(2110)$ and $f_1(2210)$, and $f_1(2310)$, i.e.,

TABLE IX. Obtained ratios for decays of $b_1(1960)$. All results correspond to $R = 4.66$–5.16 GeV^{-1}.

Ratio	Value	Ratio	Value
$\Gamma_{\pi a_0(980)}/\Gamma_{\text{Total}}$	0.186–0.235	$\Gamma_{\rho\rho}/\Gamma_{\text{Total}}$	0.028–0.031
$\Gamma_{\pi\omega_{1420}}/\Gamma_{\text{Total}}$	0.088–0.107	$\Gamma_{\omega\pi}/\Gamma_{\text{Total}}$	0.077–0.162
$\Gamma_{\rho\rho}/\Gamma_{\pi a_2(1320)}$	0.572–0.624	$\Gamma_{KK^*(892)}/\Gamma_{\eta\rho}$	0.648–0.736
$\Gamma_{\rho f_0}/\Gamma_{\pi a_1(1260)}$	0.029–0.030	$\Gamma_{KK_1(1400)}/\Gamma_{KK_1(1270)}$	0.249–0.316

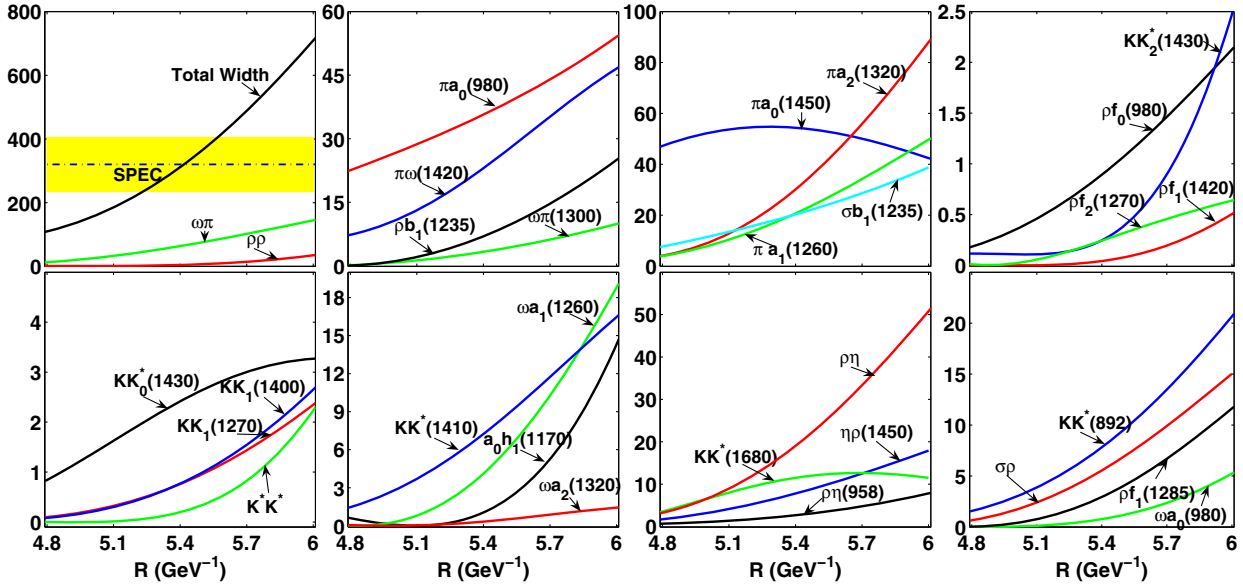

FIG. 10 (color online). R dependence of the calculated partial and total decay widths of $b_1(2240)$. Here, the dot-dashed line with the band is the experimental total width from Ref. [12]. We do not present the $K^*K_1(1270)$ contribution since this decay has a tiny width. All results are in units of MeV.

$$\begin{pmatrix} |f_1(1970)\rangle \\ |f_1(2110)\rangle \end{pmatrix} = \begin{pmatrix} \cos\phi_2 & -\sin\phi_2 \\ \sin\phi_2 & \cos\phi_2 \end{pmatrix} \begin{pmatrix} |n\bar{n}\rangle \\ |s\bar{s}\rangle \end{pmatrix} \tag{9}$$

and

$$\begin{pmatrix} |f_1(2210)\rangle \\ |f_1(2310)\rangle \end{pmatrix} = \begin{pmatrix} \cos\phi_3 & -\sin\phi_3 \\ \sin\phi_3 & \cos\phi_3 \end{pmatrix} \begin{pmatrix} |n\bar{n}\rangle \\ |s\bar{s}\rangle \end{pmatrix}. \tag{10}$$

Here, the mixing angles $\phi_i (i = 1, 2, 3)$ cannot be constrained by our analysis. In the following discussions, we take a typical value $\phi_i = \phi = 24°$ to give the quantitative results.

As for $f_1(1285)$, we show its partial and total decay widths in Fig. 11, where the calculated total decay width is in agreement with the experimental data from Ref. [67]. However, we notice that the calculated branching ratio for $\Gamma_{\pi a_0}/\Gamma_{\text{total}} = 0.67$–$0.68$, corresponding to $R = (3.00$–$4.00)$ GeV^{-1}, which is a little bit larger than $(36 \pm 7)\%$ listed in the PDG [1]. The PDG data also shows that the branching ratio of its decay $\eta\pi\pi$ can reach up to $(52.4^{+1.9}_{-2.2})\%$ [1], which is the main contribution to the total decay width of $f_1(1285)$. In this work, we study the processes $f_1(1285) \to \eta\sigma \to \eta\pi\pi$ and $f_1(1285) \to \pi a_0(980) \to \eta\pi\pi$, which can be calculated using the QPC model. Thus, the decay width of $f_1(1285) \to \eta\sigma \to \eta\pi\pi$ can be written as [44]

$$\Gamma(f_1 \to \eta + \sigma \to \eta + \pi\pi) = \frac{1}{\pi}\int_{4m_\pi^2}^{(m_{f_1}-m_\eta)^2} dr\sqrt{r}\frac{\Gamma_{f_1\to\eta+\sigma}(r)\cdot\Gamma_{\sigma\to\pi\pi}(r)}{(r-m_\sigma^2)^2+(m_\sigma\Gamma_\sigma)^2}, \tag{11}$$

TABLE X. Calculated ratios for $b_1(2240)$ corresponding to $R = 5.20$–5.54 GeV^{-1}.

Ratio	Value	Ratio	Value
$\Gamma_{\pi a_0(980)}/\Gamma_{\text{Total}}$	0.097–0.128	$\Gamma_{\pi a_0(1450)}/\Gamma_{\text{Total}}$	0.131–0.232
$\Gamma_{\pi\omega_{1420}}/\Gamma_{\text{Total}}$	0.068–0.071	$\Gamma_{\omega\pi}/\Gamma_{\text{Total}}$	0.179–0.199
$\Gamma_{\pi a_2(1320)}/\Gamma_{\text{Total}}$	0.075–0.102	$\Gamma_{\pi a_1(1260)}$	0.057–0.066
$\Gamma_{\eta\rho(1450)}/\Gamma_{\text{Total}}$	0.055–0.064	$\Gamma_{\eta\rho}/\Gamma_{\text{Total}}$	0.050–0.062
$\Gamma_{KK^*(1680)}/\Gamma_{\text{Total}}$	0.042–0.057	$\Gamma_{\rho f_1(1285)}/\Gamma_{\omega a_1(1260)}$	0.678–0.819
$\Gamma_{\rho f_0}/\Gamma_{\rho b_1(1235)}$	0.112–0.173	$\Gamma_{\rho f_2(1270)}/\Gamma_{KK_1(1400)}$	0.254–0.317
$\Gamma_{KK_1(1270)}/\Gamma_{KK_0^*(1430)}$	0.233–0.383	$\Gamma_{\rho\eta'(958)}/\Gamma_{KK^*(1410)}$	0.364–0.381
$\Gamma_{KK^*(1410)}/\Gamma_{KK^*(892)}$	0.903–0.950	$\Gamma_{\omega a_0(980)}/\Gamma_{\omega a_1(1260)}$	0.158–0.204

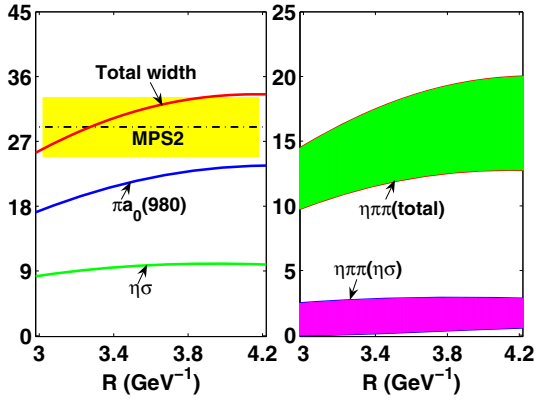

FIG. 11 (color online). R dependence of the total and partial decay widths of $f_1(1285)$. We also present the decay width of $f_1(1285) \to \eta\pi\pi$ via the intermediate channels $\eta\sigma$ and $\pi a_0(980)$ (green band), and only from the intermediate channel $\eta\sigma$ (pink band). Here, the experimental total width from Ref. [67] is denoted by the dot-dashed line with the band. All results are in units of MeV.

where the interaction of σ with two pions can be described by the effective Lagrangian

$$\mathcal{L}_{\sigma\pi\pi} = g_\sigma \sigma(2\pi^+\pi^- + \pi^0\pi^0). \tag{12}$$

The coupling constant $g_\sigma = 2.12$–2.81 GeV is determined by the total width $\Gamma_\sigma = 400 \sim 700$ MeV [1], and the decay width reads as

$$\Gamma_{\sigma\to\pi\pi}(r) = \frac{g_\sigma^2\lambda^2}{8\pi r}\frac{[(r-(2m_\pi)^2)r]^{1/2}}{2\sqrt{r}}, \tag{13}$$

where $\lambda = \sqrt{2}$ and 1 for $\pi^+\pi^-$ and $\pi^0\pi^0$, respectively.

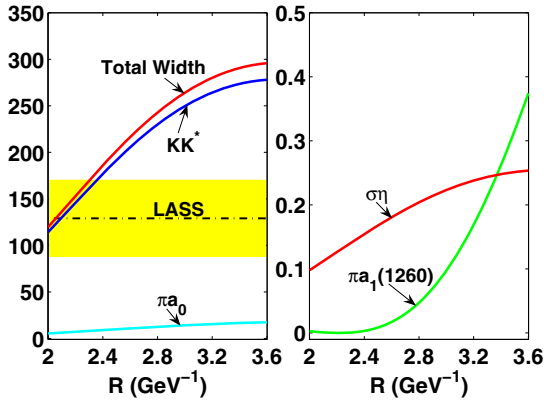

FIG. 12 (color online). R dependence of the total and partial decay widths of $f_1(1420)$. Here, the experimental total width from Ref. [68] is shown by the dot-dashed line with the band. All results are in units of MeV.

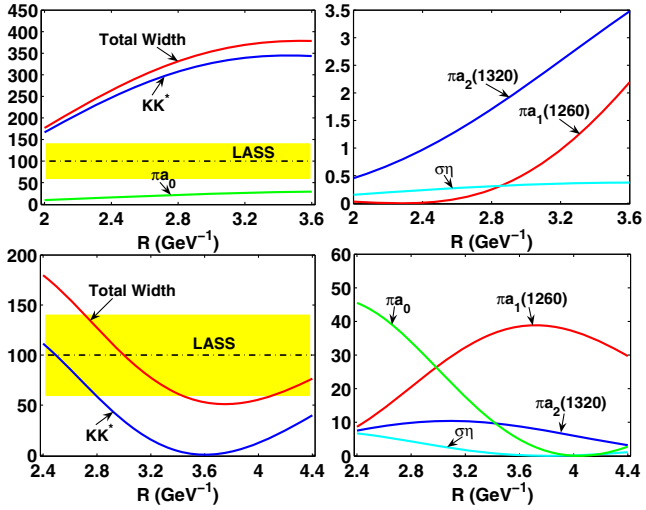

FIG. 13 (color online). Total and partial decay widths of $f_1(1510)$ as a partner of $f_1(1285)$ (first row) and as the first radial excitation of $f_1(1285)$ (second row). The experimental total width from Ref. [69] is denoted by the dot-dashed line with the band. All results are in units of MeV.

The process $f_1(1285) \to \pi a_0(980) \to \eta\pi\pi$ is calculated in a similar way, and the equation is given by

$$\Gamma(f_1 \to a_0 + \pi \to \eta + \pi\pi) = \frac{1}{\pi}\int_{(m_\pi+m_\eta)^2}^{(m_{f_1}-m_\pi)^2} dr\sqrt{r}\frac{\Gamma_{f_1\to\pi+a_0}(r)\cdot\Gamma_{a_0\to\eta\pi}(r)}{(r-m_{a_0}^2)^2+(m_{a_0}\Gamma_{a_0})^2}, \tag{14}$$

where the decay width for $a_0(980) \to \eta\pi$ is

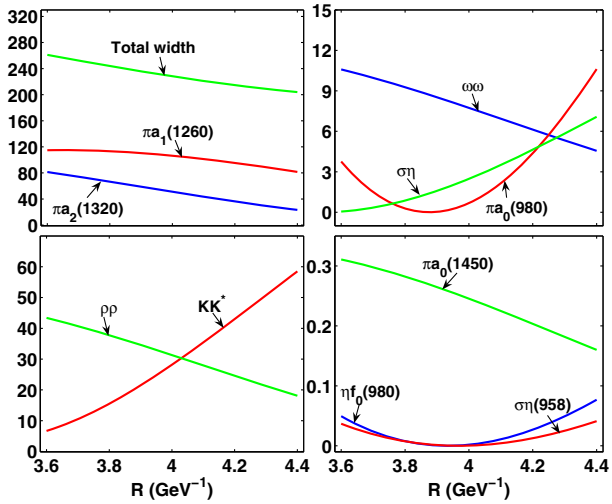

FIG. 14 (color online). R dependence of the total and partial decay widths of $f_1(1640)$. All results are in units of MeV.

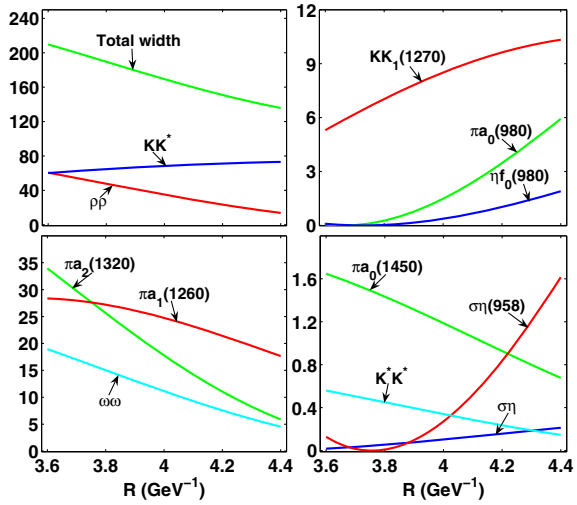

FIG. 15 (color online). R dependence of the total and partial decay widths of $f_1(1800)$. All results are in units of MeV.

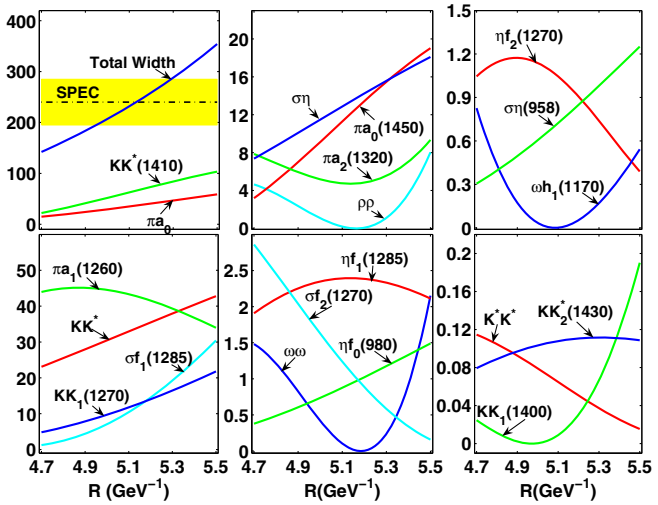

FIG. 16 (color online). R dependence of the total and partial decay widths of $f_1(1970)$. The experimental total width from Ref. [24] is denoted by the dot-dashed line with the band. All results are in units of MeV.

$$\Gamma_{a_0(980)\to\eta\pi}(r) = \frac{g_{a_0}^2}{8\pi r}\frac{[(r-(m_\eta+m_\pi)^2)(r-(m_\eta-m_\pi))^2]^{1/2}}{2\sqrt{r}}, \quad (15)$$

where the coupling constant $g_{a_0} = 1.262$–2.524 GeV is determined by the total width of $a_0(980)(\Gamma_{a_0(980)} = 50$–$100$ MeV). The final result of the width of $f_1(1285) \to \pi a_0(980) \to \eta\pi\pi$ includes the contributions from both $\eta\pi^0\pi^0$ and $\eta\pi^+\pi^-$.

The decay width of $f_1(1285) \to \eta\pi\pi$ via both the intermediate $\eta\sigma$ and $\pi a_0(980)$ channels and only the intermediate $\eta\sigma$ channel are shown in Fig. 11. In addition, the decay width of $f_1(1285) \to \eta\pi\pi$ from the intermediate $\pi a_0(980)$ channel is comparable with the corresponding experimental data $[(16 \pm 7)\%]$ in the PDG [1].

In the following, we discuss the decay behaviors of $f_1(1420)$ and $f_1(1510)$ as partners of $f_1(1285)$. As for $f_1(1420)$, the obtained total decay width can overlap with the DM2 result [68], as shown in Fig. 12. Its main decay channel is KK^*. Thus, the present study of decay of $f_1(1420)$ supports the prediction that $f_1(1420)$ is a partner of $f_1(1285)$. As for $f_1(1510)$, its partial and total decay widths are listed in Fig. 13, which shows that the calculated total decay width is larger than the experimental data [68]. Thus, the possibility that $f_1(1510)$ is a partner of $f_1(1285)$ can be excluded.

In Figs. 14 and 15, we further illustrate the decay properties of the two predicted states $f_1(1640)$ and $f_1(1800)$. In addition, we also list some of their typical ratios, which are weakly dependent on the R value (see Table XI), where we take $R = (3.60$–$4.40)$ GeV^{-1}. From Figs. 14 and 15 and Table XI, we can obtain information on the main decay modes and the resonance parameters of the two predicted f_1 mesons.

As for $f_1(1510)$, there also exists another possible assignment, i.e., $f_1(1510)$ can be a radial excitation of $f_1(1285)$ since the mass of $f_1(1510)$ is close to that of the predicted $f_1(1640)$. Here, we use the mixing angle expression

$$|f_1(1510)\rangle = \cos\phi_1|n\bar{n}\rangle - \sin\phi_1|s\bar{s}\rangle, \quad (16)$$

which is the same as $f_1(1640)$. Thus, we also further illustrate the decay behavior of $f_1(1510)$ as a radial excitation of $f_1(1285)$ (see Fig. 13). Under this assignment, the obtained total decay width can be fitted with the LASS data [69]. The KK^* mode also has a large contribution to the total decay width. These facts indicate the possibility that $f_1(1510)$ is a radial excitation of $f_1(1285)$.

In Fig. 16, we show the R dependence of the decay behavior of $f_1(1970)$ as the second radial excitation of $f_1(1285)$. Its main decay channels are $KK^*(1410)$, $\pi a_0(980)$, $\pi a_1(1260)$, and KK^*. As a partner of

TABLE XI. Some obtained ratios relevant to decays of $f_1(1640)$ and $f_1(1800)$. All values correspond to the R range $(3.60$–$4.40)$ GeV^{-1}.

$f_1(1640)$		$f_1(1800)$	
$\Gamma_{\pi a_1(1260)}/\Gamma_{\text{Total}}$	0.400–0.440	$\Gamma_{\rho\rho}/\Gamma_{\text{Total}}$	0.102–0.290
$\Gamma_{\pi a_2(1320)}/\Gamma_{\text{Total}}$	0.114–0.312	$\Gamma_{\omega\omega}/\Gamma_{\pi a_1(1260)}$	0.254–0.665
$\Gamma_{\omega\omega}/\Gamma_{\rho\rho}$	0.244–0.254	$\Gamma_{KK_1(1270)}/\Gamma_{KK^*}$	0.088–0.141
$\Gamma_{KK^*}/\Gamma_{\text{Total}}$	0.026–0.284	$\Gamma_{\pi a_2(1320)}/\Gamma_{\text{Total}}$	0.043–0.162

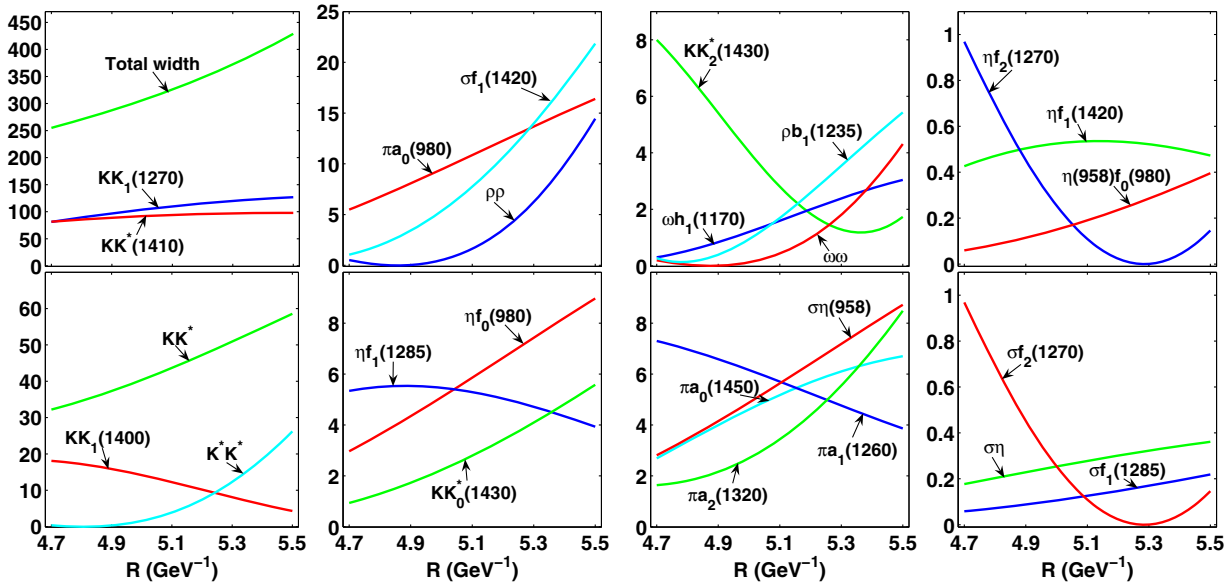

FIG. 17 (color online). R dependence of the total and partial decay widths of $f_1(2110)$. All results are in units of MeV.

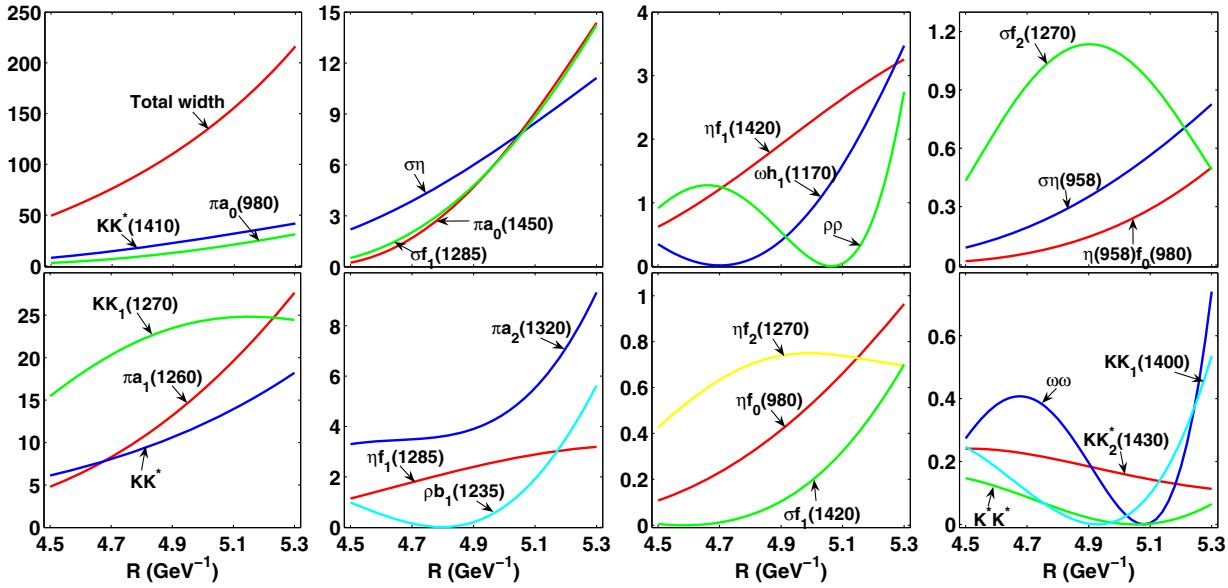

FIG. 18 (color online). R dependence of the total and partial decay widths of $f_1(2210)$. All results are in units of MeV.

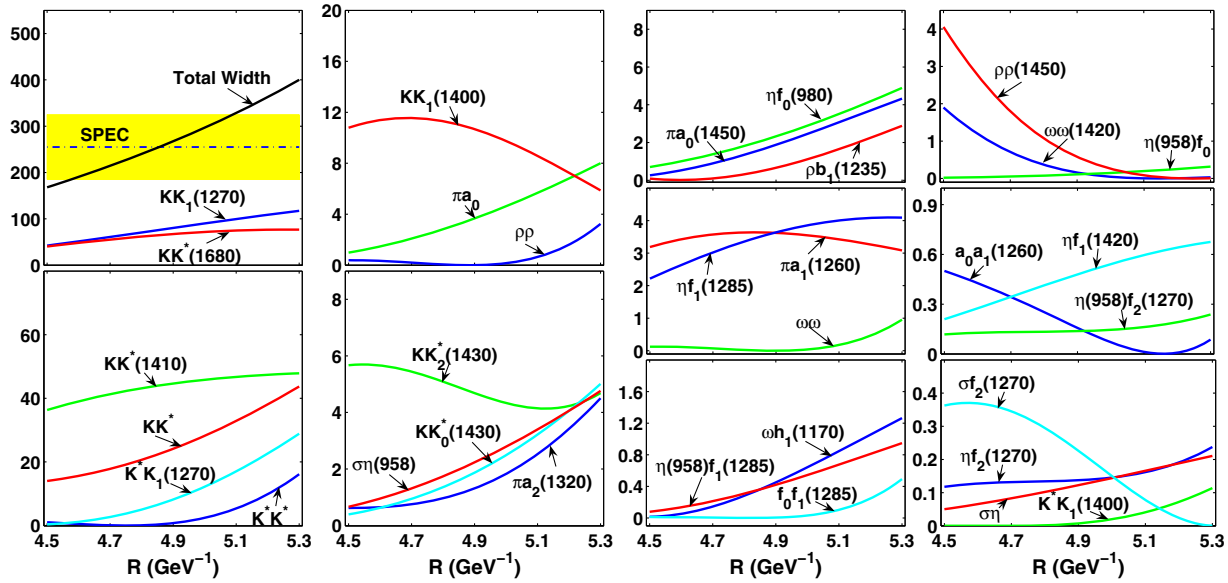

FIG. 19 (color online). R dependence of the total and partial decay widths of $f_1(2310)$. The experimental total width from Ref. [24] is denoted by the dot-dashed line with the band. All results are in units of MeV.

$f_1(1970)$, the predicted $f_1(2110)$ mainly decays into $KK_1(1270)$, $KK^*(1410)$, and KK^* and has a large total decay width, as shown in Fig. 17.

The third radial excitation of $f_1(1285)$ is still missing in experiments. In this work, we predict $f_1(2210)$, and we calculate its total and partial decay widths (see Fig. 18). As a partner of this predicted $f_1(2210)$, $f_1(2310)$ has the decay properties listed in Fig. 19, in which the experimental width [24] is depicted by our calculation when taking

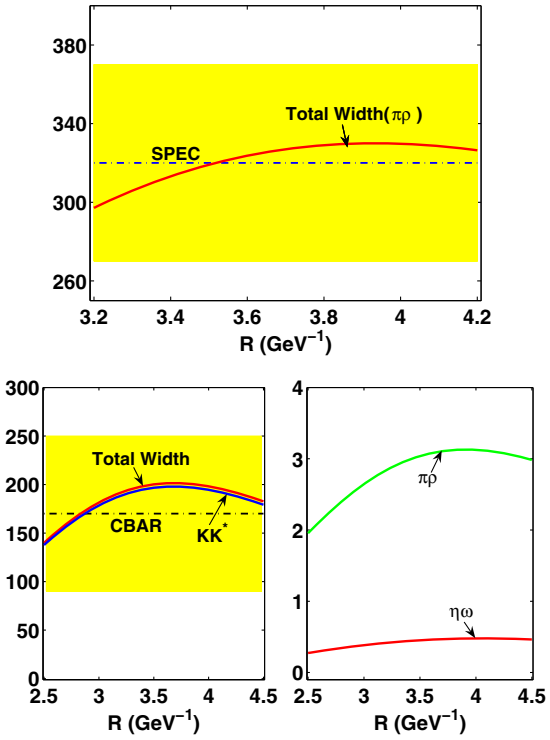

FIG. 20 (color online). R dependence of the total decay width of $h_1(1170)$ (top) and $h_1(1380)$ (bottom). Here, the dot-dashed lines with the band are from Refs. [25,28]. All results are in units of MeV.

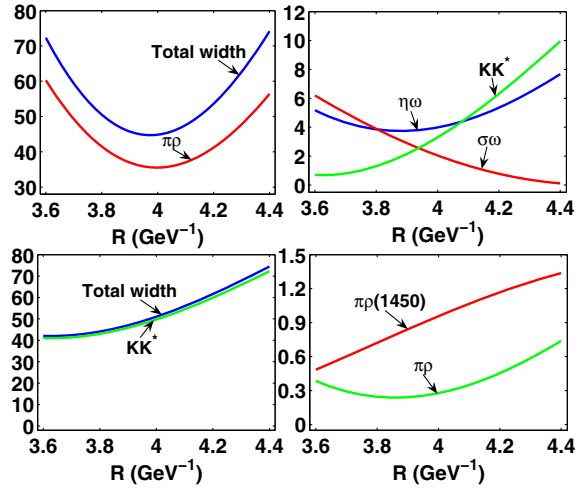

FIG. 21 (color online). R dependence of the total and partial decay widths of $h_1(1595)$ (top) and $h_1(1780)$ (bottom). All results are in units of MeV.

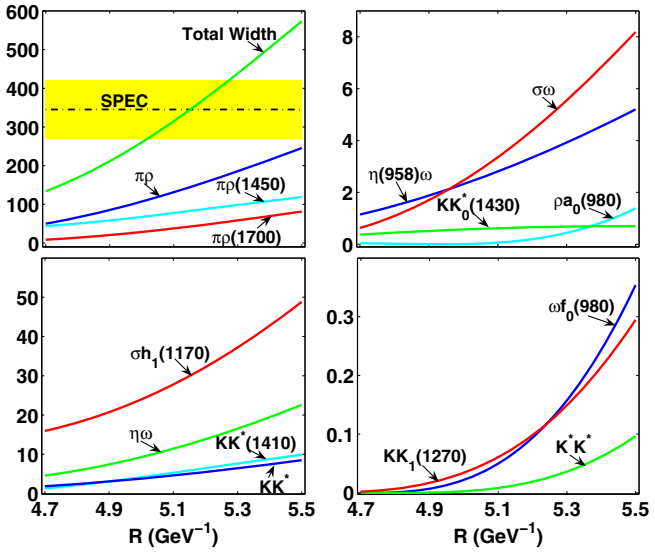

FIG. 22 (color online). R dependence of the total and partial decay widths of $h_1(1965)$. The experimental total width from Ref. [30] is denoted by the dot-dashed line with the band. All results are in units of MeV.

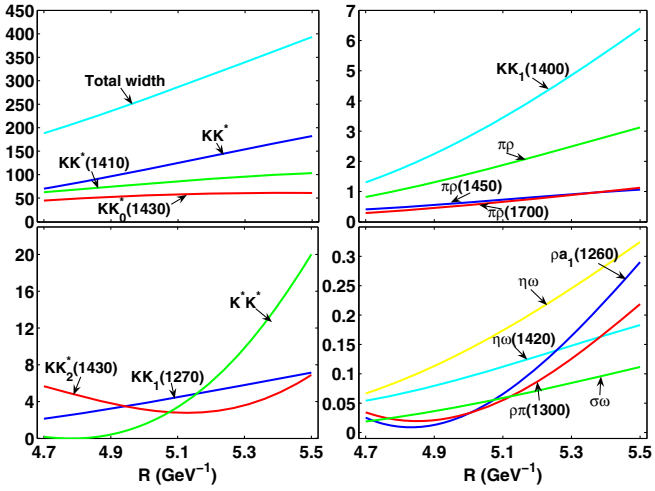

FIG. 23 (color online). R dependence of the total and partial decay widths of $h_1(2120)$. All results are in units of MeV.

$R = (4.58\text{–}5.10)$ GeV^{-1}. Its main decay channels are $KK_1(1270)$, $KK^*(1680)$, $KK^*(1410)$, and KK^*.

D. h_1 states

Similar to the f_1 mesons, the following study of h_1 states is relevant to the admixtures of the flavor wave functions $n\bar{n}$ and $s\bar{s}$. As the ground states in the h_1 meson family, $h_1(1170)$ and $h_1(1380)$ satisfy

$$\begin{pmatrix} |h_1(1170)\rangle \\ -|h_1(1380)\rangle \end{pmatrix} = \begin{pmatrix} \sin\theta_1 & \cos\theta_1 \\ -\cos\theta_1 & \sin\theta_1 \end{pmatrix} \begin{pmatrix} |n\bar{n}\rangle \\ |s\bar{s}\rangle \end{pmatrix}, \quad (17)$$

where the mixing angle θ_1 is introduced, the first line of this equation is adopted in this paper, and the second line is used in Ref. [70]. In Ref. [70], Cheng obtained $\theta_1 \sim 82.7°$. The lattice QCD calculation indicates $\theta_1 = 86.8°$ [71]. In addition, $\theta_1 = 85.6°$ was obtained in Ref. [72]. In our calculation, we present our result as $\theta_1 = 85.6°$.

The obtained partial and total decay widths of $h_1(1170)$ and $h_1(1380)$ are shown in Fig. 20. Our results indicate that $h_1(1170)$ and $h_1(1380)$ are suitable candidates for the ground states in the h_1 meson family. Our result that $h_1(1380)$ mainly decays into KK^* is consistent with the experimental fact that $h_1(1380)$ has a dominant $s\bar{s}$ component [21,28].

According to the Regge trajectory analysis in Fig. 1, $h_1(1595)$, $h_1(1965)$, and $h_1(2215)$ are the first, second, and third radial excitations of $h_1(1170)$. Here, $h_1(1595)$, $h_1(1965)$, and $h_1(2215)$ have the same flavor wave functions as $h_1(1170)$ in Eq. (17). The mixing angle θ_1 in Eq. (17) is replaced by θ_2, θ_3, and θ_4 for the corresponding h_1 states. As for these higher radial excitations, the mixing angles θ_i $(i = 2, 3, 4)$ were not well determined. Thus, we take a typical mixing angle $\theta_i = 85.6°$ to discuss the decay behaviors of $h_1(1595)$, $h_1(1965)$, and $h_1(2215)$.

As for $h_1(1595)$, we find that the obtained total decay width is much smaller than $384 \pm 60^{+70}_{-100}$ MeV measured by the BNL-E852 Collaboration [29]. Thus, we suggest performing a precise measurement of the resonance parameters of $h_1(1595)$, which would be helpful in clarifying this discrepancy. The result shown in Fig. 21 indicates that $\pi\rho$ is a dominant decay mode of $h_1(1595)$. In addition, $h_1(1595) \to \omega\eta$ has a sizable contribution to the total decay width, which explains why the $\omega\eta$ mode was found in Ref. [73]. As the predicted partner of $h_1(1595)$, $h_1(1780)$ dominantly decays into KK^*, as presented in Fig. 21.

Figure 22 presents the results for $h_1(1965)$, where the calculated total decay width can overlap with the Crystal Barrel data [30] when $R = (5.02\text{–}5.28)$ GeV^{-1}. Its main decay channels are $\pi\rho$, $\pi\rho(1450)$, and $\pi\rho(1700)$, while $\sigma h_1(1170)$ also provides a considerable value. As a partner of $h_1(1965)$, $h_1(2120)$ is predicted in this work, where its main decay modes are KK^*, $KK^*(1410)$, and $KK_0^*(1430)$ (see Fig. 23 for more details on its decay properties).

The total and partial decay widths of $h_1(2215)$ and its partner $h_1(2340)$ predicted in this work are listed in Figs. 24 and 25, respectively. The main decay modes of $h_1(2215)$ and $h_1(2340)$ can be found in Figs. 24 and 25.

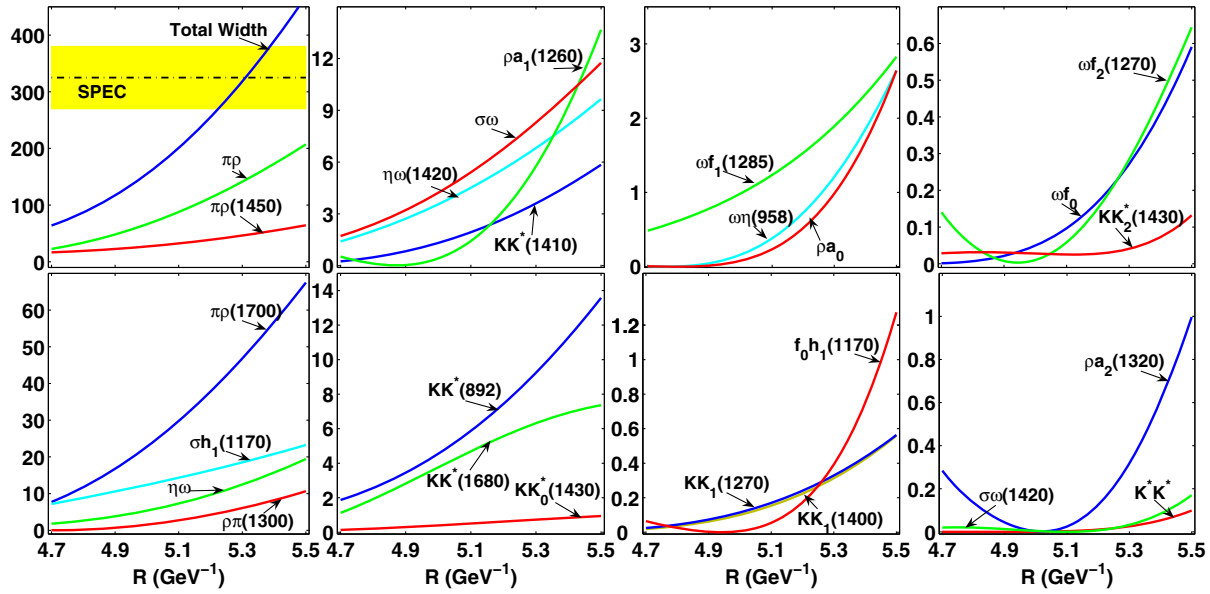

FIG. 24 (color online). R dependence of the total decay width of $h_1(2215)$. The experimental total width from Ref. [30] is denoted by the dot-dashed line with the band. All results are in units of MeV.

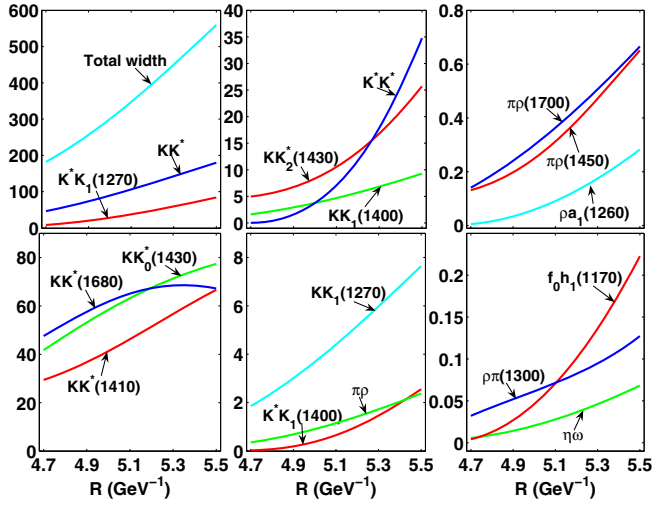

FIG. 25 (color online). R dependence of the total decay width of $h_1(2340)$. All results are in units of MeV.

III. DISCUSSION AND CONCLUSION

Although there are abundant axial-vector states in the PDG [1], the properties of the observed axial-vector states are still unclear. The present unsatisfactory research status of the observed axial-vector states stimulates us to systematically study them, which will be helpful for revealing their underlying structures. As a crucial step, we have studied whether the observed axial-vector states can be categorized into the axial-vector meson family.

In this work, we have discussed the observed axial-vector states by assigning them as conventional states in the axial-vector meson family, where both the analysis of the mass spectra and the calculation of their two-body OZI-allowed strong decays have been performed.

In our calculation using the QPC model, we took different R ranges to reproduce the total width of the discussed axial-vector states. For the a_1 and b_1 states, for example, we listed the obtained R values for different states (see Table XII for more details). We found that the corresponding R values become larger with an increase in the radial quantum number, which is consistent with our understanding, i.e., the size of higher radial excitations is larger than that of lower radial excitations. Thus, our calculation can reflect this phenomenon, which provides a test of the reliability of our calculation. In addition, we also noticed that states with the same radial quantum number in the a_1 and b_1 families have similar R ranges, which reflects the fact that the a_1 state is the isospin partner of the corresponding b_1 state.

When we discussed the decay behaviors of higher radial excitations in the f_1 and h_1 meson families, we fixed the corresponding mixing angles to match the numerical results, which is due to the absence of a theoretical study

TABLE XII. The obtained R values for the a_1 and b_1 states discussed in this work.

state	$n^{2S+1}L_J$	$R\,(\mathrm{GeV}^{-1})$	state	$n^{2S+1}L_J$	$R\,(\mathrm{GeV}^{-1})$
$a_1(1260)$	1^3P_1	3.846	$b_1(1235)$	1^1P_1	3.704
$a_1(1640)$	2^3P_1	4.30–4.64	$b_1(1640)$	2^1P_1	
$a_1(1930)$	3^3P_1	4.58–4.92	$b_1(1960)$	3^1P_1	4.66–5.16
$a_1(2095)$	3^3P_1	4.78–5.16			
$a_1(2270)$	4^3P_1	5.12–5.32	$b_1(2240)$	4^1P_1	5.20–5.54

of these mixing angles, and these mixing angles cannot be determined by the present experimental data [1]. However, for the ground states of f_1 and h_1, the situation is totally different, where the corresponding mixing angles are fixed by experimental data. Thus, in this work we adopted a very simple and crude approach, i.e., we took the same value of the mixing angle for the ground and the corresponding radial excitations. We expect more experimental data on radial excitations in the f_1 and h_1 meson families. Then we can carry out further theoretical studies by considering the effect of the mixing angles.

In summary, this phenomenological analysis not only tested possible assignments of the axial-vector states, but also predicted abundant information about their partial decays, which is valuable for further experimental studies of the observed states. In addition, we have also predicted some missing axial-vector mesons, and have roughly determined their mass values and decay behaviors. We have also suggested an experimental search for the missing states; the BESIII and COMPASS experiments will be good platforms to carry out the study of light hadron spectra.

ACKNOWLEDGMENTS

This project is supported by the National Science Foundation for Fostering Talents in Basic Research of the National Natural Science Foundation of China and the National Natural Science Foundation of China under Grants No. 11222547 and No. 11175073, the Ministry of Education of China (SRFDP under Grant No. 2012021111000), and the Fok Ying Tung Education Foundation (Grant No. 131006).

[1] K. A. Olive *et al.* (Particle Data Group Collaboration), Chin. Phys. C **38**, 090001 (2014).
[2] D. Barberis *et al.* (WA102 Collaboration), Phys. Lett. B **507**, 14 (2001).
[3] D. M. Asner *et al.* (CLEO Collaboration), Phys. Rev. D **61**, 012002 (1999).
[4] S. U. Chung *et al.*, Phys. Rev. D **65**, 072001 (2002).
[5] C. A. Baker *et al.*, Phys. Lett. B **449**, 114 (1999).
[6] D. V. Amelin *et al.* (VES Collaboration), Phys. Lett. B **356**, 595 (1995).
[7] A. V. Anisovich, C. A. Baker, C. J. Batty, D. V. Bugg, V. A. Nikonov, A. V. Sarantsev, V. V. Sarantsev, and B. S. Zou, Phys. Lett. B **517**, 261 (2001).
[8] J. Kuhn *et al.* (E852 Collaboration), Phys. Lett. B **595**, 109 (2004).
[9] U. Karshon, G. Mikenberg, Y. Eisenberg, S. Pitluck, E. E. Ronat, A. Shapira, and G. Yekutieli, Phys. Rev. D **10**, 3608 (1974).
[10] C. Amsler *et al.* (Crystal Barrel Collaboration), Phys. Lett. B **311**, 362 (1993).
[11] M. Nozar *et al.* (E852 Collaboration), Phys. Lett. B **541**, 35 (2002).
[12] A. V. Anisovich, C. A. Baker, C. J. Batty, D. V. Bugg, L. Montanet, V. A. Nikonov, A. V. Sarantsev, V. V. Sarantsev, and B. S. Zou, Phys. Lett. B **542**, 8 (2002).
[13] D. Barberis *et al.* (WA102 Collaboration), Phys. Lett. B **471**, 440 (2000).
[14] V. Dorofeev *et al.*, Eur. Phys. J. A **47**, 68 (2011).
[15] M. J. Corden *et al.*, Nucl. Phys. **B144**, 253 (1978).
[16] A. Gurtu *et al.* (Amsterdam-CERN-Nijmegen-Oxford Collaboration), Nucl. Phys. **B151**, 181 (1979).
[17] T. Bolton *et al.*, Phys. Lett. B **278**, 495 (1992).
[18] D. Barberis *et al.* (WA102 Collaboration), Phys. Lett. B **440**, 225 (1998).
[19] C. Bromberg *et al.*, Phys. Rev. D **22**, 1513 (1980).
[20] C. Dionisi *et al.* (CERN-College de France-Madrid-Stockholm Collaboration), Nucl. Phys. **B169**, 1 (1980).
[21] D. Aston *et al.*, Phys. Lett. B **201**, 573 (1988).
[22] A. Birman *et al.*, Phys. Rev. Lett. **61**, 1557 (1988); **62**, 1577 (E) (1989).
[23] M. Ablikim *et al.* (BESIII Collaboration), Phys. Rev. Lett. **106**, 072002 (2011).
[24] A. V. Anisovich, C. A. Baker, C. J. Batty, D. V. Bugg, C. Hodd, H. C. Lu, V. A. Nikonov, A. V. Sarantsev, V. V. Sarantsev, and B. S. Zou, Phys. Lett. B **491**, 47 (2000).
[25] J. A. Dankowych *et al.*, Phys. Rev. Lett. **46**, 580 (1981).
[26] M. Atkinson *et al.* (Omega Photon and Bonn-CERN-Glasgow-Lancaster-Manchester-Paris-Rutherford-Sheffield Collaborations), Nucl. Phys. **B231**, 15 (1984).
[27] A. Ando *et al.*, Phys. Lett. B **291**, 496 (1992).
[28] A. Abele *et al.* (Crystal Barrel Collaboration), Phys. Lett. B **415**, 280 (1997).
[29] P. Eugenio *et al.* (BNL-E852 Collaboration), Phys. Lett. B **497**, 190 (2001).
[30] A. V. Anisovich, C. A. Baker, C. J. Batty, D. V. Bugg, L. Montanet, V. A. Nikonov, A. V. Sarantsev, V. V. Sarantsev, and B. S. Zou, Phys. Lett. B **542**, 19 (2002).
[31] A. V. Anisovich, V. V. Anisovich, and A. V. Sarantsev, Phys. Rev. D **62**, 051502 (2000).
[32] L. Micu, Nucl. Phys. **B10**, 521 (1969).
[33] A. Le Yaouanc, L. Oliver, O. Pene, and J. C. Raynal, Phys. Lett. B **72**, 57 (1977).
[34] A. Le Yaouanc, L. Oliver, O. Pene, and J.-C. Raynal, Phys. Lett. B **71**, 397 (1977).
[35] A. Le Yaouanc, L. Oliver, O. Pene, and J. C. Raynal, Phys. Rev. D **11**, 1272 (1975).
[36] A. Le Yaouanc, L. Oliver, O. Pene, and J.-C. Raynal, Phys. Rev. D **9**, 1415 (1974).
[37] A. Le Yaouanc, L. Oliver, O. Pene, and J. C. Raynal, Phys. Rev. D **8**, 2223 (1973).

[38] E. S. Ackleh, T. Barnes, and E. S. Swanson, Phys. Rev. D **54**, 6811 (1996).
[39] H. G. Blundell, arXiv:hep-ph/9608473.
[40] R. Bonnaz, B. Silvestre-Brac, and C. Gignoux, Eur. Phys. J. A **13**, 363 (2002).
[41] H. Q. Zhou, R. G. Ping, and B. S. Zou, Phys. Lett. B **611**, 123 (2005).
[42] J. Lu, W.-Z. Deng, X.-L. Chen, and S.-L. Zhu, Phys. Rev. D **73**, 054012 (2006).
[43] B. Zhang, X. Liu, W. Z. Deng, and S. L. Zhu, Eur. Phys. J. C **50**, 617 (2007).
[44] Z.-G. Luo, X.-L. Chen, and X. Liu, Phys. Rev. D **79**, 074020 (2009).
[45] Z. F. Sun and X. Liu, Phys. Rev. D **80**, 074037 (2009).
[46] X. Liu, Z. G. Luo, and Z. F. Sun, Phys. Rev. Lett. **104**, 122001 (2010).
[47] Z. F. Sun, J. S. Yu, X. Liu, and T. Matsuki, Phys. Rev. D **82**, 111501 (2010).
[48] T. A. Rijken, M. M. Nagels, and Y. Yamamoto, Nucl. Phys. **A835**, 160 (2010).
[49] C.-Q. Pang, L.-P. He, X. Liu, and T. Matsuki, Phys. Rev. D **90**, 014001 (2014).
[50] B. Wang, C. Q. Pang, X. Liu, and T. Matsuki, Phys. Rev. D **91**, 014025 (2015).
[51] Z.-C. Ye, X. Wang, X. Liu, and Q. Zhao, Phys. Rev. D **86**, 054025 (2012).
[52] X. Wang, Z. F. Sun, D. Y. Chen, X. Liu, and T. Matsuki, Phys. Rev. D **85**, 074024 (2012).
[53] L.-P. He, X. Wang, and X. Liu, Phys. Rev. D **88**, 034008 (2013).
[54] Y. Sun, X. Liu, and T. Matsuki, Phys. Rev. D **88**, 094020 (2013).
[55] E. van Beveren, C. Dullemond, and G. Rupp, Phys. Rev. D **21**, 772 (1980); **22**, 787(E) (1980).
[56] E. van Beveren, G. Rupp, T. A. Rijken, and C. Dullemond, Phys. Rev. D **27**, 1527 (1983).
[57] S. Capstick and W. Roberts, Phys. Rev. D **49**, 4570 (1994).
[58] P. R. Page, Nucl. Phys. **B446**, 189 (1995).
[59] A. I. Titov, T. I. Gulamov, and B. Kampfer, Phys. Rev. D **53**, 3770 (1996).
[60] M. Jacob and G. C. Wick, Ann. Phys. (N.Y.) **7**, 404 (1959); **281**, 774 (2000).
[61] J.-S. Yu, Z.-F. Sun, X. Liu, and Q. Zhao, Phys. Rev. D **83**, 114007 (2011).
[62] R. R. Akhmetshin *et al.* (CMD2 Collaboration), Phys. Lett. B **466**, 392 (1999).
[63] P. Weidenauer *et al.* (ASTERIX. Collaboration), Z. Phys. C **59**, 387 (1993).
[64] F. E. Close and A. Kirk, Z. Phys. C **76**, 469 (1997).
[65] R. Aaij *et al.* (LHCb Collaboration), Phys. Rev. Lett. **112**, 091802 (2014).
[66] J. J. Dudek, R. G. Edwards, P. Guo, and C. E. Thomas, Phys. Rev. D **88**, 094505 (2013).
[67] J. H. Lee *et al.*, Phys. Lett. B **323**, 227 (1994).
[68] J. E. Augustin *et al.* (DM2 Collaboration), Phys. Rev. D **46**, 1951 (1992).
[69] H. Aihara *et al.* (TPC/Two Gamma Collaboration), Phys. Rev. D **38**, 1 (1988).
[70] H. Y. Cheng, Phys. Lett. B **707**, 116 (2012).
[71] J. J. Dudek, R. G. Edwards, B. Joó, M. J. Peardon, D. G. Richards, and C. E. Thomas, Phys. Rev. D **83**, 111502 (2011).
[72] D. M. Li, B. Ma, and H. Yu, Eur. Phys. J. A **26**, 141 (2005).
[73] A. V. Anisovich, C. A. Baker, C. J. Batty, D. V. Bugg, V. A. Nikonov, A. V. Sarantsev, V. V. Sarantsev, and B. S. Zou, Phys. Lett. B **507**, 23 (2001).